Chapter 5

Synthesis, characterization, *In vitro* anti-cancer evaluation, ADMET properties and molecular docking of novel quinoline - isoxazole hybrids

5.1 Introduction

The Wittig reaction, introduced by Georg Wittig in 1954,[153] is a cornerstone in organic chemistry for the synthesis of alkenes.[154] The Wittig reaction is a widely used method in organic synthesis for converting aldehydes and ketones into alkenes using a phosphonium ylide.[155] This reaction involves a [2+2] cycloaddition followed by a ring opening to produce the alkene product.[156] Wittig's discovery earned him the Nobel Prize in Chemistry in 1979 due to the reaction's transformative impact on organic synthesis.[157] This method is celebrated for its ability to precisely control the geometry (cis or trans) of the resulting double bond, making it a valuable tool for synthesizing complex organic molecules, particularly in pharmaceuticals and material science.[158] The Wittig reagent (phosphonium ylide) is produced by deprotonating a phosphonium salt with a strong base.[159] The ylide subsequently attacks the carbonyl carbon of an aldehyde or ketone, resulting in the formation of a betaine intermediate, which then cyclizes to yield an oxaphosphetane, a four-membered ring comprising oxygen and phosphorus.[160,161] The oxaphosphetane experiences ring opening, facilitated by the establishment of a robust P=O bond, resulting in the synthesis of the alkene and triphenylphosphine oxide.[162] Stabilized ylides, characterized by electron-withdrawing groups such as esters or nitriles, preferentially yield the *E*-isomer owing to thermodynamic control. Unstabilized ylides preferentially form the *Z*-isomer owing to kinetic control.[163]

Conversely, Isoxazole's ability to engage in several non-bonding interactions has been shown to be linked to a variety of biological processes.[164] The broad range of biological activities exhibited by the oxazole substances indicate their ability to connect with a number of enzymes and receptors in biological systems[165] including anti-bacterial,[166] anti-fungal,[167] anti-viral,[168] anti-tubercular,[169] anti-cancer,[170] and anti-inflammatory activities.[171] The marketed quinoline-based cancer therapy medications and their molecular targets like cabozantinib (**1**, Thyroid cancer) viz. Non-specific tyrosine kinase inhibitor,[172] neratinib (**2**, Breast cancer) viz. tyrosine kinase inhibitor,[173] sitamaquine (**3**, Prostate cancer) viz. inhibit heme polymerase activity,[174] quinoline analogue (**4**, Blood cancer) viz. inhibitors by cell cycle

arrest,[175] amg-208 (**5**, Prostate cancer) viz. inhibitor of hepatocyte growth factor receptor,[176] pyrazolo acridine (**6**, Liver cancer),[177] Foretinib (**7,** Breast cancer) viz. inhibitor of receptor tyrosine kinase,[178] irinotecan (**8**, Colorectal cancer) viz. topoisomerase-I,[179] amsacrine (**9**, Acute leukaemia) viz. inhibiting topoisomerase-II,[180] talazoparib (**10**, Breast cancer) viz. poly adp ribose polymerase (parp) inhibitor,[181] acridine carboxamide (**11**, Lung, Brain and CNS system tumors).[182] Many pharmaceutical substances contain isoxazole and its derivatives, which includes NVP-AUY922 (**12**, anticancer), cloxacillin (**13**, antibacterial), leflunamide (**14,** anti-inflammatory), sulfamethoxazole (**15**, antibacterial) and valdecoxib (**16**, anti-inflammatory) (**Figure 1**).

In the last twenty years, there has been a surge in interest in the synthesis of hybrid compounds[183] and their evaluation as potent pharmaceutical and therapeutic agents (**17, 18**).[184] The shuffling of two or more known pharmacophores into a single structure and a strong strategy to produce novel leads with complimentary activity constitute hybridization, a cogent technique in contemporary drug discovery.[185] In light of the aforementioned discoveries, and continuing to develop powerful anticancer drugs based on quinoline heterocyclic core,[186] in an effort to create and prepare novel hybrid compounds with quinoline cores linked by biologically strong isoxazole linkage, which have been developed as anticancer agents.

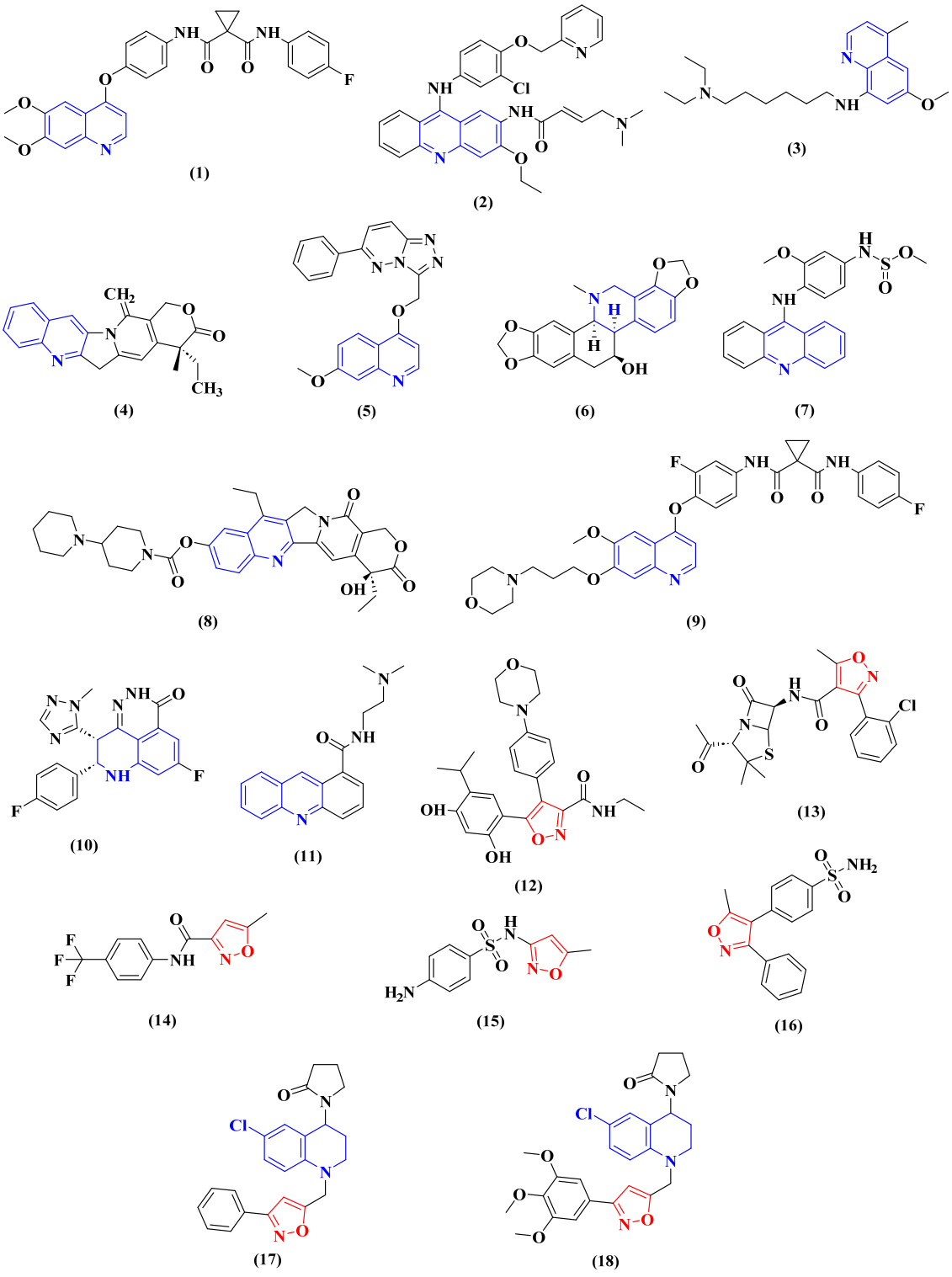

Figure 1: Quinoline and isoxazole based clinical trial drugs.

5.1.1 Synthetic methodologies for the substituted quinoline-isoxazole hybrid's framework and its biological significance

The ester functional group of compound (**1**) was converted to alcohol through treatment with diisobutylaluminium hydride (DIBAL) in toluene at 0 °C, yielding (2-chloro-4-(4-fluorophenyl)-6-isopropyl pyrimidin-5-yl)methanol (**2**). The bromination of compound (**2**) using phosphorus tribromide in DCM at 0 °C, followed by treatment with triphenyl phosphine in toluene at reflux temperature, yielded phosphorous salt (**3**), specifically triphenyl[2-chloro-{4-(4-fluorophenyl)-6-isopropyl-pyrimidin-5-yl}phosphor-ium] bromide. Following the establishment of convenient access to pyrimidine phosphonium salt (**3**), to synthesize a collection of novel (*E*)-5 styryl pyrimidines by the Wittig olefination method. Initially, compound **3** reacted with different substituted aldehydes (**4**) employing sodium tripolyphosphate in H_2O at 70 °C, to get desired compound **5** (**Figure 5.1**).[187]

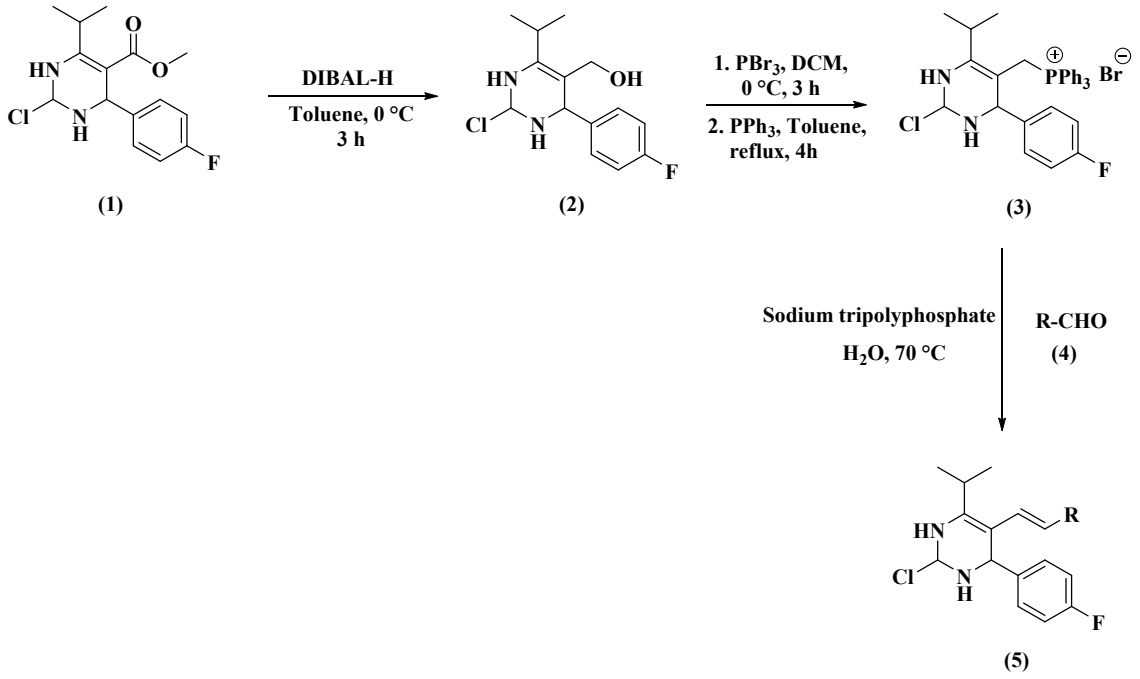

Figure 5.1

The ring-opening reaction of 3-methylthio-4-nitrothiophene (**6**) with pyrrolidine and silver nitrate, followed by S-methylation, yields 1,1-bis(methylthio)-3-nitro-4-pyrrolidino-1,3-butadiene (**8**). The treatment of this nitroenamine with arylmagnesium bromides leads to the chemoselective substitution of the pyrrolidine group with the aryl component of the Grignard

reagent. The synthesized 4-aryl-1,1-bis(methylthio)-3-nitro-1,3-butadienes (**9**) can serve as precursors for the synthesis of isoxazoles (**11**). The reduction of **9** can be achieved using lead powder in a combination of acetic acid and DMF at ambient temperature. The cyclization of vinyloximes (**10**) utilizing an acidic ion-exchange resin in acetonitrile yields the appropriate isoxazoles (**11**) (**Figure 5.2**).[188]

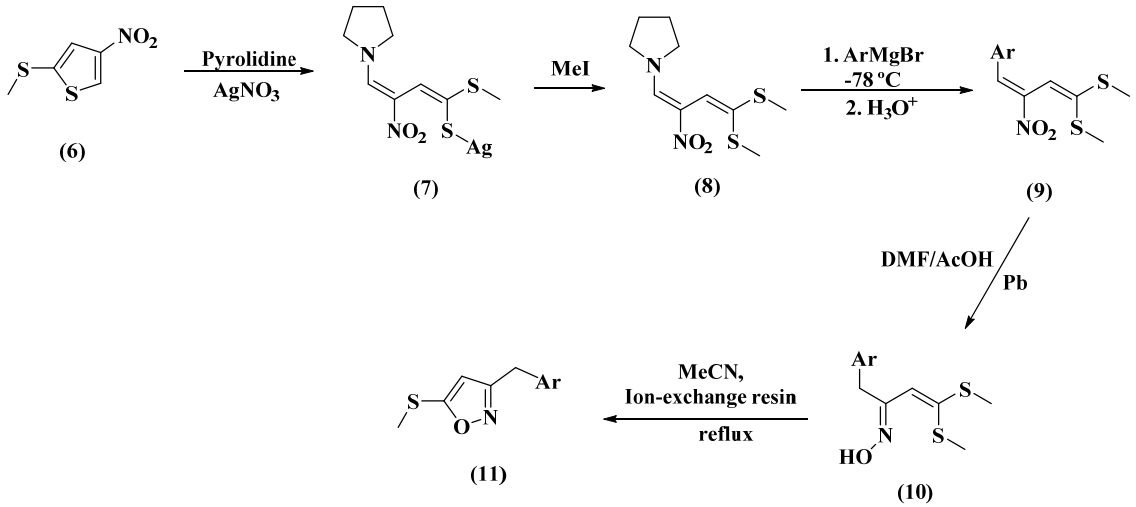

Figure 5.2

An alternate pathway to ABT-418 (**15**) has recently been delineated.[189] The oxidation-Wittig reaction of *N*-ethoxycarbonylprolinol (**12**) facilitates the manufacture of the corresponding pyrrolidine with an α,β-unsaturated ketone substituent (**13**) in 72% yield. The one-pot transformation into 3-methyl-5-(carboethoxy)pyrrolidineisoxazole (**14**), followed by $LiAlH_4$ reduction, yields the desired compound. ABT-418 is a bioactive molecule which gives numerous anticancer activities (**Figure 5.3**).[190]

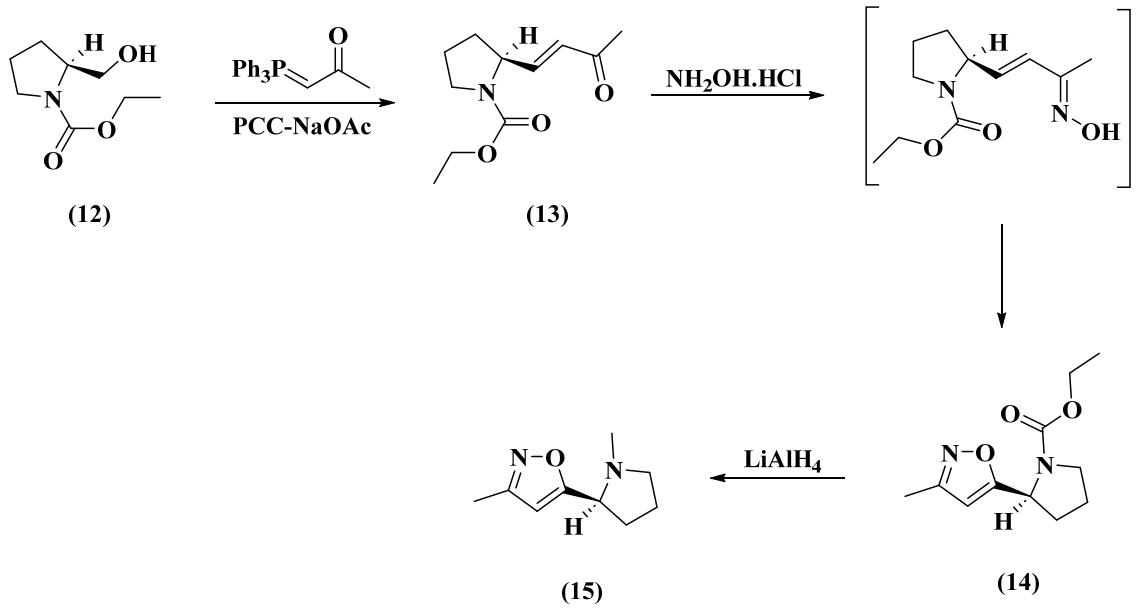

Figure 5.3

The subsequent reaction of compound **16** an intermediate sodium enolate with diethyl oxalate produced keto-enol ester **17**. The isoxazole heterocyclic compound **18** was synthesized by reacting compound **17** with hydroxylamine hydrochloride in ethanol (**Figure 5.4**).[191]

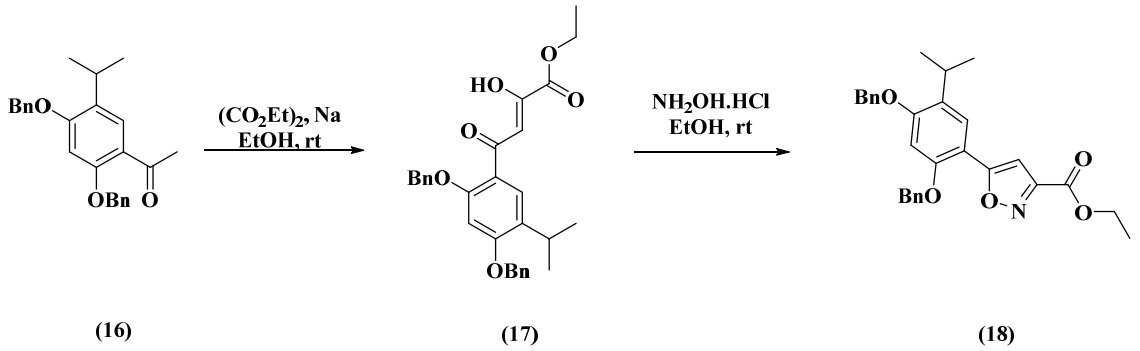

Figure 5.4

The isoxazolo[4,3-*c*]quinoline ring system (**23**) can be synthesized from *o*-azido benzonitrile oxide (**19**) through sequential cycloaddition with enolates of 1,3-dicarbonyl compounds **20**, both generated *in situ*, and an intramolecular aza-wittig reaction. The azidophenyl-isoxazoles **21** react with triphenylphosphine to yield the imino phosphoranes **22**,

which are not isolated but instead undergo direct cyclization by an intramolecular aza-wittig reaction to get targeted compound **23** (**Figure 5.5**).[192]

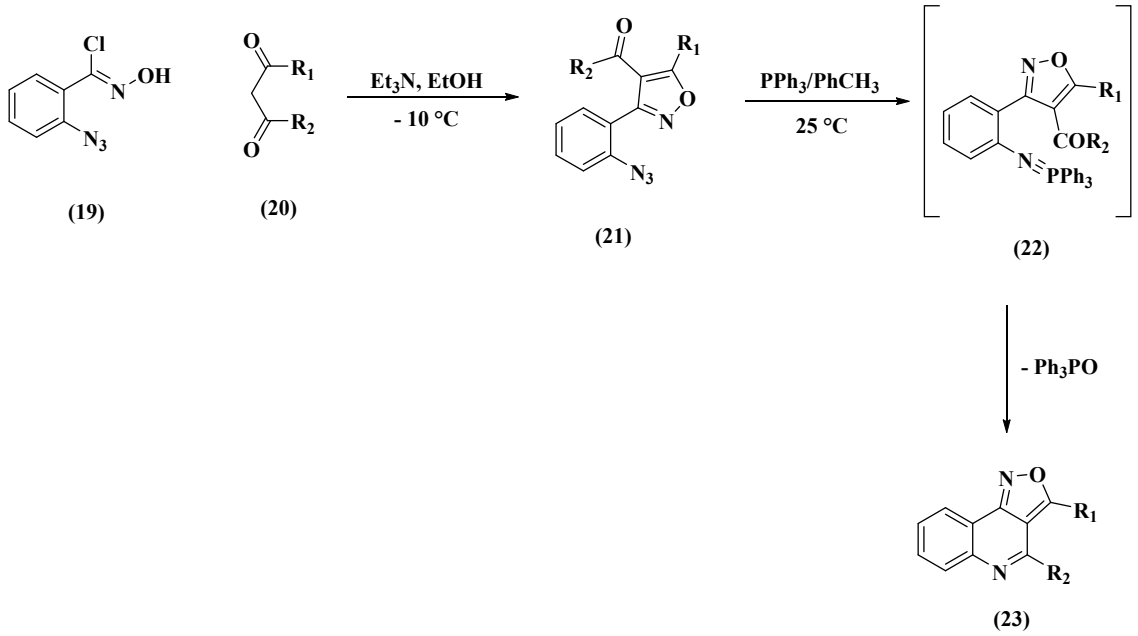

Figure 5.5

5.2 Results and Discussion

5.2.1 Chemistry

This was done in an effort to develop novel anti-cancer molecules and to synthesise various heterocyclic molecules having quinoline and isoxazole in their primary structure are reported here. Scheme **1**, illustrates the process of creating quinoline hybrid molecules with isoxazole **(7a-l)** that serve as potent anti-cancer agents. Compounds **2** to **5** synthesized previously in chapter-4. Further, compound **5** and triphenylphosphine (PPh_3) interacted in toluene at 120 °C to produce 3-(2-chloroquinolin-3-yl)-5-((triphenyl-λ^4-phosphaneyl)methyl)isoxazole **(6)**.[187] At last, compound **6** was performed in a basic condition (i.e. K_2CO_3), with substituted aryl aldehyde by using dimethyl sulfoxide (DMSO) as a solvent at room temperature to yield the quinoline containing isoxazole derivatives **(7a-l)**.[187]

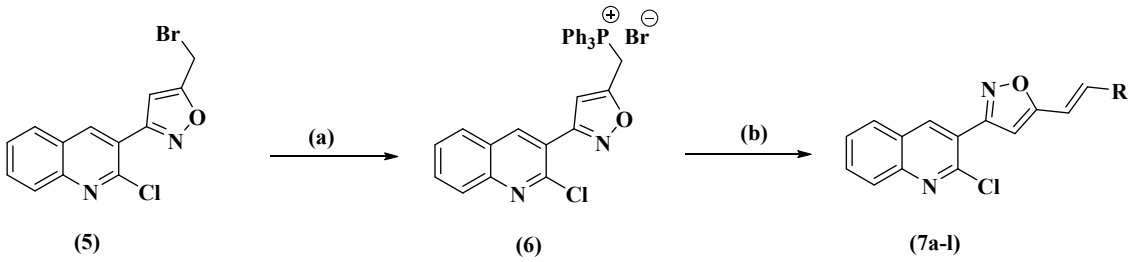

Where R = Different substituted aldehydes.

Reaction condition: a) Triphenylphosphine, Toluene 120 °C, 2h; (b) R-CHO, K_2CO_3, DMSO, rt, 2 h.

Scheme 1: Synthesis of the quinoline containing isoxazole derivatives.

Table 1: Physicochemical characteristics of the novel quinoline containing isoxazole derivatives **7a-l.**

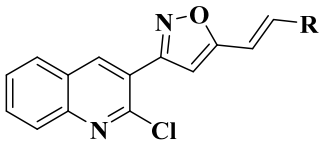

Compound	R	Molecular Weight	Molecular Formula	Yield (%)	Melting Point (°C)
7a	4-OCH_3-C_6H_4-	362.81	$C_{21}H_{15}ClN_2O_2$	93	203-205
7b	4-CH_3-C_6H_4-	346.81	$C_{21}H_{15}ClN_2O$	97	192-194
7c	3-Br-C_6H_4-	411.68	$C_{20}H_{12}BrClN_2O$	90	223-225
7d	3-OCH_3-C_6H_4-	362.81	$C_{21}H_{15}ClN_2O_2$	94	202-204
7e	3,4-OCH_3-C_6H_3-	392.84	$C_{22}H_{17}ClN_2O_3$	84	206-208
7f	4-Cl-C_6H_4-	367.23	$C_{20}H_{12}Cl_2N_2O$	92	218-220
7g	2-Cl-C_6H_4-	367.23	$C_{20}H_{12}Cl_2N_2O$	90	215-217
7h	4-F-C_6H_4-	350.78	$C_{20}H_{12}FClN_2O$	88	209-211
7i	2-OH-C_6H_4-	348.79	$C_{20}H_{13}ClN_2O_2$	96	196-198
7j	1-$C_{10}H_8$-	382.85	$C_{24}H_{15}ClN_2O$	80	205-207
7k	1-C_4H_4S	338.81	$C_{18}H_{11}ClN_2OS$	96	190-192
7l	4-Br-C_6H_4-	411.68	$C_{20}H_{12}BrClN_2O$	96	226-228

5.3 Biological Activity:

5.3.1 In vitro study for anticancer activity

In vitro cell-based screening at a single dose is the first step in the search for the cytotoxic activity of novel derivatives.[193] Compound **5** and synthesized novel hybrid compounds **7a-l** were selected for the anti-cancer screening for single dose response study by the national cancer institute (NCI/NIH), under USA's Developmental Therapeutics Programme (DTP). According to their analysis of the association between structural activity and their *in vitro* anticancer cell-line investigation. Under conventional conditions for experiments, one dosage response parameter (GI_{50}) was determined for each of the 60 human tumour cell lines (NCI-60),[194] representing nine cell line panels like leukemia, non-small-cell lung cancer, colon cancer, CNS cancer, melanoma, ovarian cancer, renal cancer, prostate cancer, and breast cancer cell lines were employed. Initially, the anti-tumor outcomes of targeted compounds indicate that compounds **5**, **7f** and **7h** shows very promising biological screening responses against GI_{50} values. Table **1** depicted the most active compound's comparable response against the 60 cell line panels (NCI-60).

Table 1. Growth % of sub-panels of tumour cell at single dose assay for compounds **5**, **7f** and **7h**.

Compounds	**5**	**7f**	**7h**
Cell line	***Growth of Cells (%)^3 10^{-5} M***		
Leukemia			
CCRF-CEM	**-38.01**	68.08	88.56
HL-60(TB)	**-48.30**	100.75	110.13
K-562	**-20.00**	56.42	86.59
MOLT-4	**-34.43**	55.73	86.06
RPMI-8226	**-36.15**	40.61	36.80
SR	**-64.15**	NT[a]	NT
NSCL Cancer			
A549/ATCC	61.26	**0.13**	25.22
EKVX	**-81.34**	27.37	69.22
HOP-62	104.39	8.70	47.53
HOP-92	21.31	**-12.16**	26.70
NCI-H226	40.32	**-67.26**	**-40.44**

NCI-H23	**-66.13**	25.48	37.72
NCI-H322M	108.03	7.12	27.57
NCI-H460	88.82	**-25.68**	7.78
NCI-H522	**-82.04**	54.76	74.36
Colon Cancer			
COLO 205	**-65.12**	31.73	65.64
HCC-2998	19.69	50.26	62.49
HCT-116	1.57	22.19	20.60
HCT-15	**-78.43**	45.11	67.87
HT29	NT	24.55	37.10
KM12	84.06	34.45	50.94
SW-620	**-75.96**	23.22	57.99
CNS Cancer			
SF-268	**-34.34**	39.25	42.45
SF-295	9.06	**3.50**	38.25
SF-539	1.85	15.04	9.09
SNB-19	35.50	21.83	30.32
SNB-75	54.70	**-28.06**	**-5.29**
U251	11.44	**-7.79**	9.11
Melanoma			
LOX IMVI	**-80.81**	12.69	25.78
MALME-3M	**-50.02**	38.63	62.53
M14	27.08	57.93	69.68
MDA-MB-435	16.49	66.84	68.79
SK-MEL-2	44.73	61.98	91.74
SK-MEL-28	**-80.99**	61.48	80.93
SK-MEL-5	**-5.32**	43.35	63.23
UACC-257	81.84	77.09	90.91
UACC-62	18.44	60.15	71.60
Ovarian Cancer			
IGROV1	**-5.47**	25.53	35.09
OVCAR-3	**-94.32**	2.70	31.15
OVCAR-4	**-43.13**	**-28.74**	**-15.23**
OVCAR-5	**-85.90**	25.98	46.20
OVCAR-8	**-7.52**	22.83	34.03
NCI/ADR-RES	**-33.70**	16.29	14.95

SK-OV-3	135.61	23.38	55.89
Renal Cancer			
786-0	NT	**-41.51**	11.49
A498	123.68	**-12.61**	74.12
ACHN	**-97.45**	**-79.01**	**-19.35**
CAKI-1	**-94.15**	**2.78**	45.09
RXF 393	**-34.01**	**-8.40**	32.83
SN12C	**-69.60**	**-2.46**	31.45
TK-10	**-69.49**	**-36.58**	43.04
UO-31	**-77.89**	**-76.65**	**-49.31**
Prostate Cancer			
PC-3	26.73	49.12	66.37
DU-145	46.23	53.29	52.08
Breast Cancer			
MCF7	**-42.29**	45.82	63.40
MDA-MB-231/ATCC	**-77.92**	**-43.73**	**-9.08**
HS 578T	45.08	36.47	38.97
BT-549	62.69	81.72	68.96
T-47D	**-27.20**	19.08	52.00
MDA-MB-468	139.30	**-15.14**	20.32
Mean	**-6.75**	**19.59**	**42.71**

[a]NT= Not tested

The anti-tumor outcomes of targeted compounds indicates that, compound **5** (**D – 846681**) which has bromomethyl at isoxazole's fifth position and compounds with electron windrowing group **7f** (*p*-Cl), (**D - 848061**) and compound **7h** (*p*-F), (**D - 848062**) display promising anti-cancer screening as GI_{50} values.

Further, these three compounds were selected for their five dose screening. For every cell line tested, the response parameters GI_{50} (Required molar concentration to inhibit 50% of the growth of cancer cell lines), TGI (Required molar concentration leads to total growth inhibition) and LC_{50} (Required molar concentration necessary to kill 50% of the cells) are used to illustrate the findings of the five dose screening of all nine derivatives. The compounds listed in Table **2** demonstrated moderate to good anticancer activities against all evaluated subpanel tumour cell lines at the GI_{50}, TGI, LC_{50}. Compound **5** showed promising values at GI_{50} against all the cell-line with highest value **-5.79** in Melanoma (MALME-3M, LOX IMVI),

the most active cell-line of TGI and LC_{50} in renal cancer with the values are respectively **-5.51** and **-5.25** in ACHN with **Δ** value **1**. Compound **7f** has shown maximum GI_{50} value **-5.96** and TGI value **-5.52** in CNS cancer (SNB-75) and LC_{50} in renal cancer with the value **-5.09** in ACHN. Also, compound **7f** has the highest **Δ** value **1.02** in LC_{50}. Compound **7h** having highest GI_{50} value as **-5.83** in CNS cancer (SNB-75). In TGI and GI_{50} **7h** shown topmost values are respectively **-5.02** and **-4.47** in CNS cancer (SNB-75) (**Table 2**). The dose-response curves of compounds **5**, **7f**, and **7h** against each subpanel of tumor cell lines are presented via graphically in figures **1**, **2** and **3** respectivley.

Table 2. *In vitro* anticancer activity of five dose assays for compounds **5**, **7f** and **7h**.

Panel/Cell lines	Log GI_{50} [a]	Log TGI [b]	Log LC_{50} [c]	Log GI_{50} [a]	Log TGI [b]	Log LC_{50} [c]	Log GI_{50} [a]	Log TGI [b]	Log LC_{50} [c]
	5			**7f**			**7h**		
Leukemia									
CCRF-CEM	-5.29	-4.50	-4.00	>-4.00	>-4.00	>-4.00	>-4.00	>-4.00	>-4.00
HL-60(TB)	-5.11	-4.39	-4.00	>-4.00	>-4.00	>-4.00	>-4.00	>-4.00	>-4.00
K-562	-5.49	-4.60	-4.00	-5.61	-5.21	>-4.00	-5.35	>-4.00	>-4.00
MOLT-4	-5.43	-4.24	-4.00	-5.62	>-4.00	>-4.00	>-4.00	>-4.00	>-4.00
RPMI-8226	-5.30	-4.32	-4.00	-5.37	>-4.00	>-4.00	-5.01	>-4.00	>-4.00
SR	-5.54	>-4.00	-4.00	-5.24	>-4.00	>-4.00	>-4.00	>-4.00	>-4.00
NSCL cancer									
A549/ATCC	-4.70	-4.33	>-4.00	-5.66	-5.25	>-4.00	-5.37	-4.69	-4.08
EKVX	-4.78	-4.49	-4.20	-5.31	>-4.00	>-4.00	-4.51	>-4.00	>-4.00
HOP-62	-4.76	-4.43	-4.10	-5.67	-5.14	-4.36	-5.19	-4.67	-4.24
HOP-92	-5.02	-4.54	-4.06	-5.83	-5.25	>-4.00	-5.66	-4.99	-4.09
NCI-H226	-4.85	-4.46	-4.07	-5.60	-4.93	>-4.00	-5.06	-4.59	-4.16
NCI-H23	-4.93	-4.59	-4.25	-5.36	>-4.00	>-4.00	-5.05	-4.35	>-4.00
NCI-H322M	-4.84	-4.55	-4.26	-5.50	>-4.00	>-4.00	-4.94	>-4.00	>-4.00
NCI-H460	-4.76	-4.44	-4.13	-5.61	-5.19	>-4.00	-5.36	-4.68	-4.01
NCI-H522	-5.41	-4.81	-4.31	-5.15	>-4.00	>-4.00	-4.83	-4.22	>-4.00
Colon Cancer									

COLO 205	-5.51	-5.00	-4.33	-5.46	>-4.00	>-4.00	-4.91	>-4.00	>-4.00
HCC-2998	-4.82	-4.54	-4.26	-5.05	>-4.00	>-4.00	-4.61	>-4.00	>-4.00
HCT-116	-5.23	-4.67	-4.21	-5.50	>-4.00	>-4.00	-5.41	-4.56	>-4.00
HCT-15	-5.53	-4.96	-4.40	-4.98	>-4.00	>-4.00	-4.12	>-4.00	>-4.00
HT29	-5.44	-4.66	>-4.00	-5.30	>-4.00	>-4.00	-5.25	>-4.00	>-4.00
KM12	-4.84	-4.55	-4.26	-5.04	>-4.00	>-4.00	-4.73	>-4.00	>-4.00
SW-620	-5.53	-4.97	-4.35	-5.42	>-4.00	>-4.00	-4.72	>-4.00	>-4.00
CNS Cancer									
SF-268	-4.84	-4.49	-4.15	-5.15	>-4.00	>-4.00	-5.05	>-4.00	>-4.00
SF-295	-4.80	-4.53	-4.26	-5.51	-4.84	>-4.00	-5.33	-4.70	-4.22
SF-539	-4.93	-4.62	-4.31	-5.42	-4.74	-4.09	-5.38	-4.79	-4.36
SNB-19	-4.83	-4.55	-4.28	-5.35	-4.43	>-4.00	-4.98	-4.58	-4.17
SNB-75	-5.19	-4.68	-4.34	-5.96	-5.42	-4.16	-5.83	-5.02	-4.47
U251	-4.99	-4.56	-4.12	-5.68	-5.34	-5.00	-5.49	-4.89	-4.24
Melanoma									
LOX IMVI	-5.79	-5.49	-5.20	-5.48	-4.57	>-4.00	-5.28	-4.57	>-4.00
MALME-3M	-5.79	-5.47	-5.14	-5.33	>-4.00	>-4.00	-4.30	>-4.00	>-4.00
M14	-4.88	-4.53	-4.17	-4.96	>-4.00	>-4.00	-4.52	>-4.00	>-4.00
MDA-MB-435	-4.95	-4.62	-4.30	-4.82	>-4.00	>-4.00	-4.48	>-4.00	>-4.00
SK-MEL-2	-4.82	-4.50	-4.18	-4.21	>-4.00	>-4.00	-4.47	>-4.00	>-4.00
SK-MEL-28	-4.89	-4.59	-4.29	-4.68	>-4.00	>-4.00	-4.05	>-4.00	>-4.00
SK-MEL-5	-4.89	-4.59	-4.29	-4.47	>-4.00	>-4.00	-4.23	>-4.00	>-4.00
UACC-257	-4.82	-4.50	-4.18	-4.42	>-4.00	>-4.00	>-4.00	>-4.00	>-4.00

UACC-62	-4.91	-4.60	-4.30	-4.82	>-4.00	>-4.00	-4.54	>-4.00	>-4.00
Ovarian Cancer									
IGROV1	-5.65	-5.26	-4.08	-5.40	>-4.00	>-4.00	-5.21	-4.16	>-4.00
OVCAR-3	-5.18	-4.70	-4.33	-5.52	>-4.00	>-4.00	-4.81	>-4.00	>-4.00
OVCAR-4	-4.79	-4.43	-4.07	-5.58	-5.14	>-4.00	-5.38	-4.26	>-4.00
OVCAR-5	-4.80	-4.52	-4.24	-5.52	>-4.00	>-4.00	-4.92	>-4.00	>-4.00
OVCAR-8	-4.76	-4.41	-4.05	-5.45	-4.75	>-4.00	-5.05	-4.62	-4.22
NCI/ADR-RES	-4.84	-4.40	>-4.00	-5.35	>-4.00	>-4.00	-5.22	-4.40	>-4.00
SK-OV-3	-4.80	-4.52	-4.24	-5.62	-5.12	>-4.00	-5.32	-4.73	-4.20
Renal Cancer									
786-0	-4.79	-4.48	-4.17	-5.69	-5.39	-5.09	-5.40	-4.84	-4.37
A498	-4.68	-4.43	-4.19	-5.62	-5.25	-4.27	-4.83	-4.48	-4.13
ACHN	-5.77	-5.51	-5.25	-5.73	-5.41	-5.09	-5.38	-4.79	-4.33
CAKI-1	-4.86	-4.57	-4.28	-5.65	-5.02	>-4.00	-4.96	-4.39	>-4.00
RXF 393	-5.05	-4.66	-4.30	-5.58	-5.06	>-4.00	-5.36	-4.74	-4.27
SN12C	-5.40	-4.83	-4.40	-5.61	-5.09	>-4.00	-5.05	-4.26	>-4.00
TK-10	-4.72	-4.47	-4.21	-5.50	-5.13	-4.09	-5.00	-4.57	-4.14
UO-31	-4.93	-4.60	-4.27	-5.77	-5.39	>-4.00	-5.38	-4.72	-4.21
Prostate Cancer									
PC-3	-4.83	-4.40	>-4.00	-5.15	>-4.00	>-4.00	-4.62	>-4.00	>-4.00
DU-145	-4.82	-4.55	-4.27	-5.03	>-4.00	>-4.00	-4.61	>-4.00	>-4.00
Breast Cancer									
MCF7	-5.38	-4.77	-4.17	-5.29	>-4.00	>-4.00	-4.67	>-4.00	>-4.00

MDA-MB-231/ATCC	-4.84	-4.54	-4.24	-5.63	-5.18	-4.16	-5.24	-4.64	-4.16
HS 578T	-4.86	-4.23	>-4.00	-5.54	-4.31	>-4.00	-5.39	-4.38	>-4.00
BT-549	-4.93	-4.59	-4.24	-5.20	>-4.00	>-4.00	-5.23	-4.07	>-4.00
T-47D	-5.28	-4.58	>-4.00	-5.54	>-4.00	>-4.00	-5.16	>-4.00	>-4.00
MDA-MB-468	-5.75	-5.43	-5.10	-5.56	-5.05	>-4.00	-5.37	-4.53	>-4.00
MeanMG_MID[d]	**-5.07**	**-4.62**	**-4.25**	**-5.34**	**-4.46**	**-4.07**	**-4.93**	**-4.3**	**-4.07**
Delta[e]	**0.72**	**0.89**	**1**	**0.62**	**0.96**	**1.02**	**0.9**	**0.72**	**0.4**

[a]The log of the molar concentration inhibits 50% net cell growth. [b]The log of the molar concentration leads to total growth inhibition. [c]The log of the molar concentration leads to 50% net cell death. [d]Mean graph midpoint = arithmetical mean value for all tested cancer cell lines. [e]Delta is considered low if <1, moderate 1–3, high if >3.

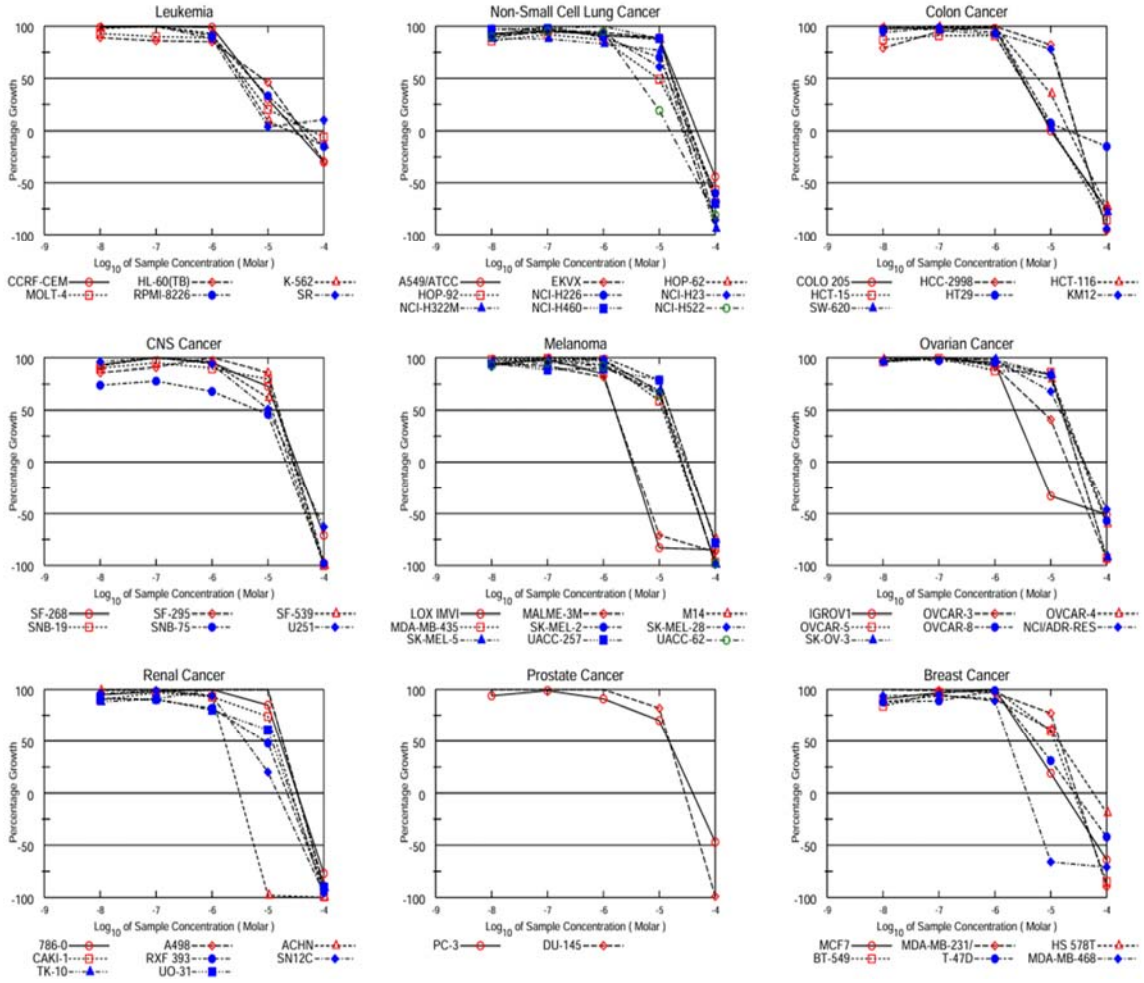

Figure 1. The dose-response curve of the active compound **5** with reference single dose and five dose values.

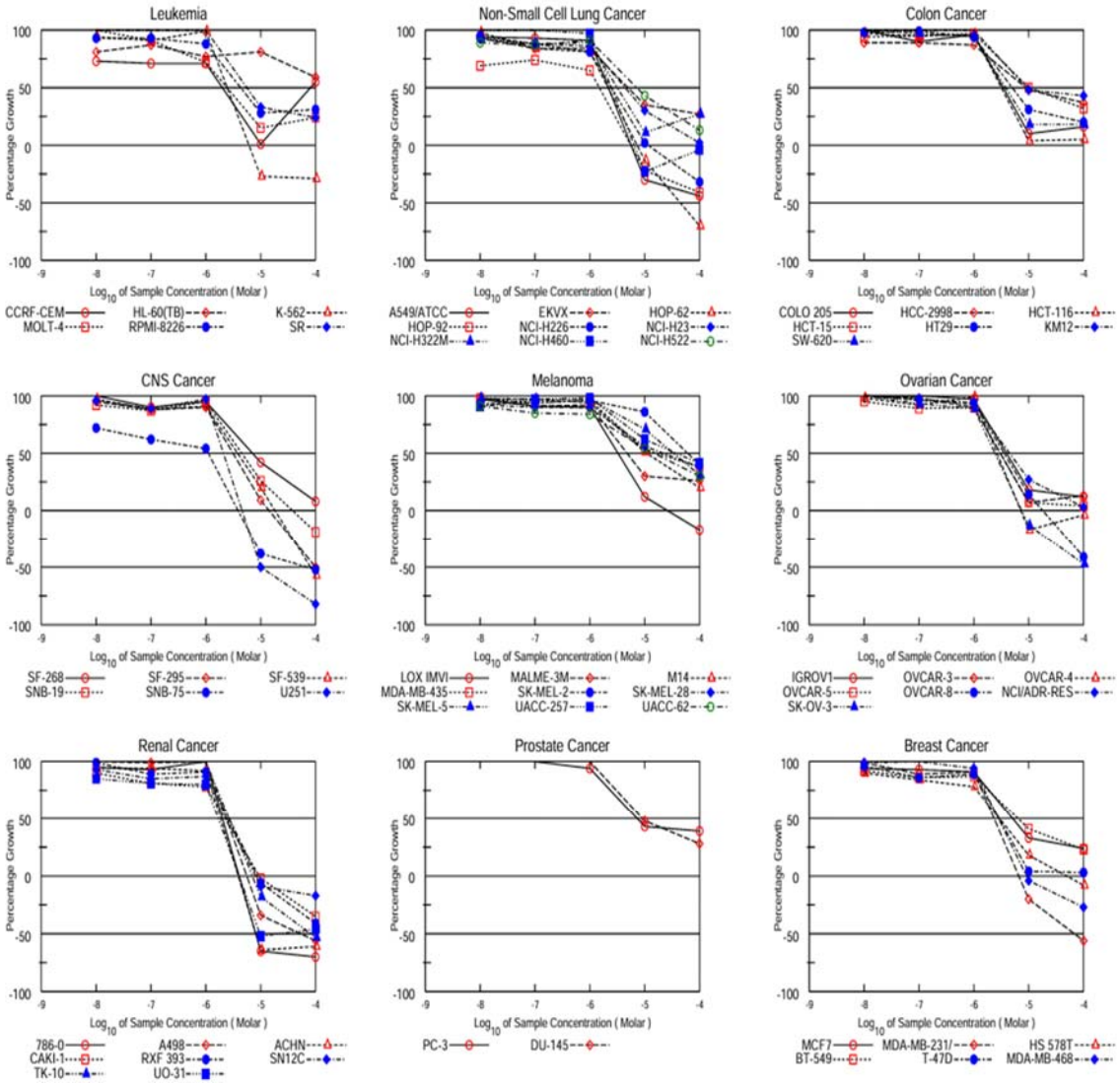

Figure 2. The dose-response curve of the active compound **7f** with reference single dose and five dose values.

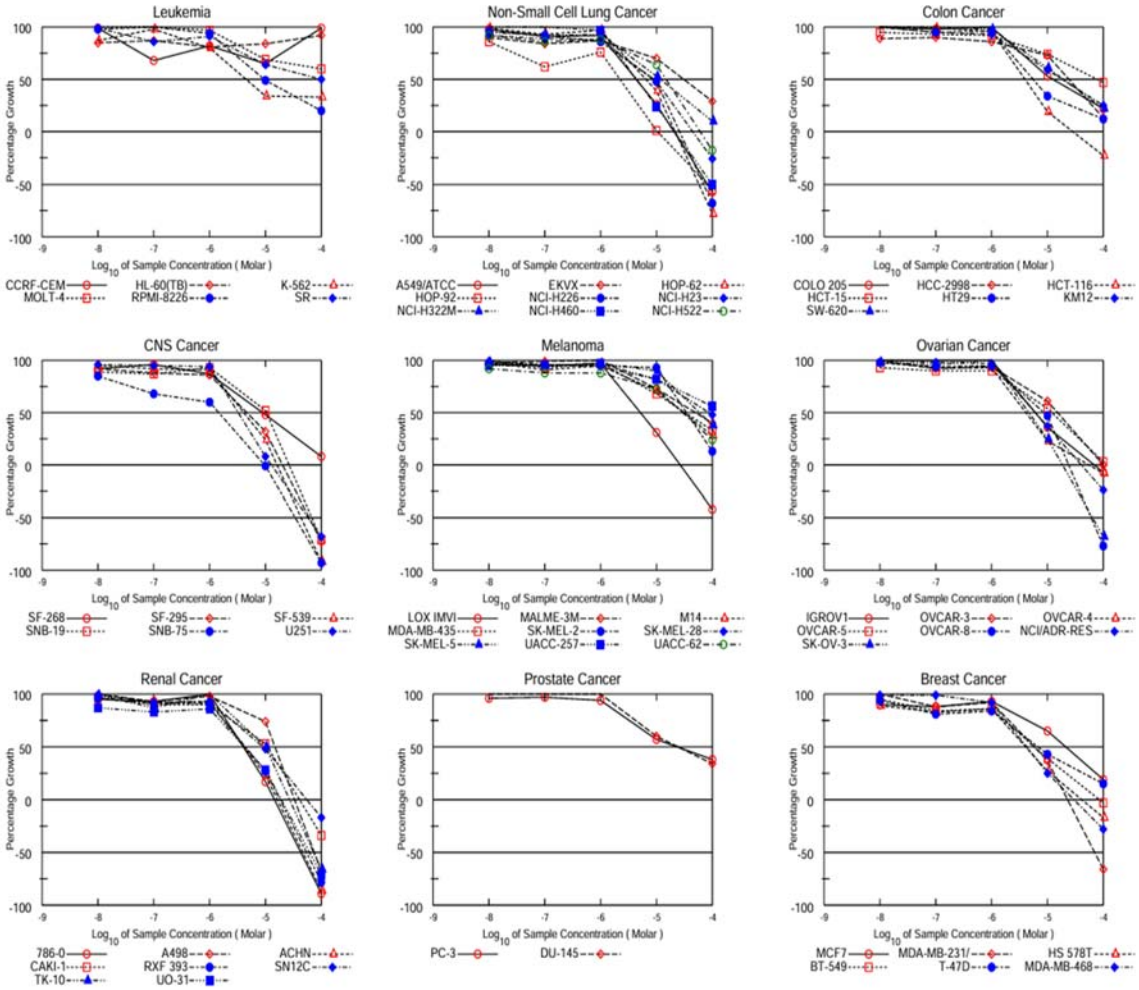

Figure 3. The dose-response curve of the active compound **7h** with reference single dose and five dose values.

5.4 Molecular Docking

In this bioinformatics study, virtual screening was performed to assess synthetic compounds for their potential to interact with the tubulin-colchicine: stathmin-like domain complex. Targeting the tubulin dynamics pathway is an appealing strategy for developing new chemotherapeutic agents.[152] Notably, the colchicine binding site within this complex is identified as a key pocket for compounds intended to disrupt tubulin polymerization. This disruption is critical because it inhibits cancer cell proliferation, making it a promising approach for cancer treatment. The study successfully identified promising compounds, **5**, **7f** and **7h** as potential inhibitors of this complex. Among all the synthetic compounds **5**, **7f** and

7h exhibits the virtuous binding affinity **-9.1**, **-9.4 & -8.9** kcal/mol respectively. The interacting residue of tubulin-colchicine: stathmin-like domain complex with **5**, **7f** and **7h** confirmed in Figure **1**, **2** and **3**. A comprehensive analysis along with types of bonds with amino acids was provided. Compound **5** formed Pi-Pi stacked bond with Trp407 (5.06 Å) & Alkyl-Pi-alkyl bon with Val181 (4.68 Å), Phe404 (4.95 Å), Val182 (3.59 Å) & Trp407 (3.84 Å, 4.59 Å). Compound **7f** formed a hydrogen bond with Gly142 (2.87 Å); Pi-alkyl bond with Ala180 (1.98 Å), Lys254 (4.60Å), Leu248 (4.05 Å); Amide π-bond with Tyr224 (3.75 Å), Gln11 (4.75 Å); Pi-sigma bond with Ala12 (3.54 Å); π-anion bond with Glu183(3.89 Å); Unfavourable donor-donor bond with Asn206(2.68 Å) & π-donor H bond with Asn101 (4.08 Å), Gly143 (3.55 Å). Whereas, while for compound **7h** conventional hydrogen bond forms with Gln11 (2.96 Å). However residue in π-alkyl bond formation with Ala250 (4.79 Å), Leu248 (4.41 Å), Lys254 (5.27 Å); Pi cation Lys254 (3.64 Å) (**Table 3**).

Table 3. Molecular docking result of novel quinoline containing isoxazole derivatives **5** and **7a-l**.

Compounds	Binding Affinity (kcal/mol)
5	-9.1
7a	-7.9
7b	-8.4
7c	-8.1
7d	-8.2
7e	-8.5
7f	-9.4
7g	-7.6
7h	-8.9
7i	-8.3
7j	-7.8
7k	-7.8
7l	-8.2
Colchicin	-6.6

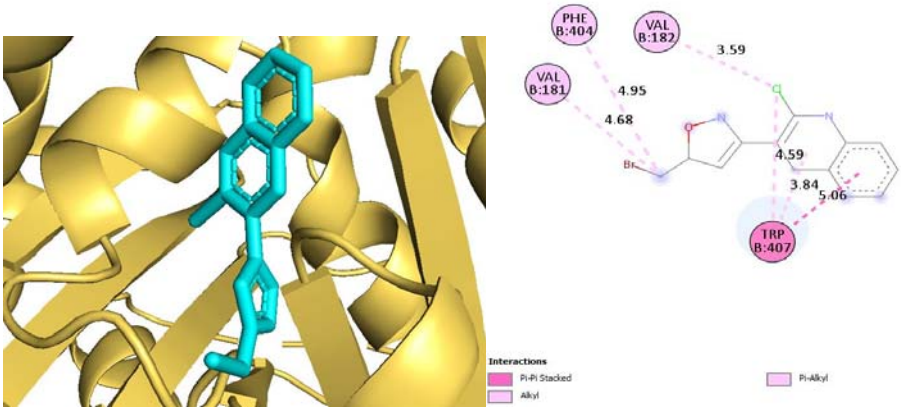

Figure 1. Best docking poses of the compound **5** with colchicin.

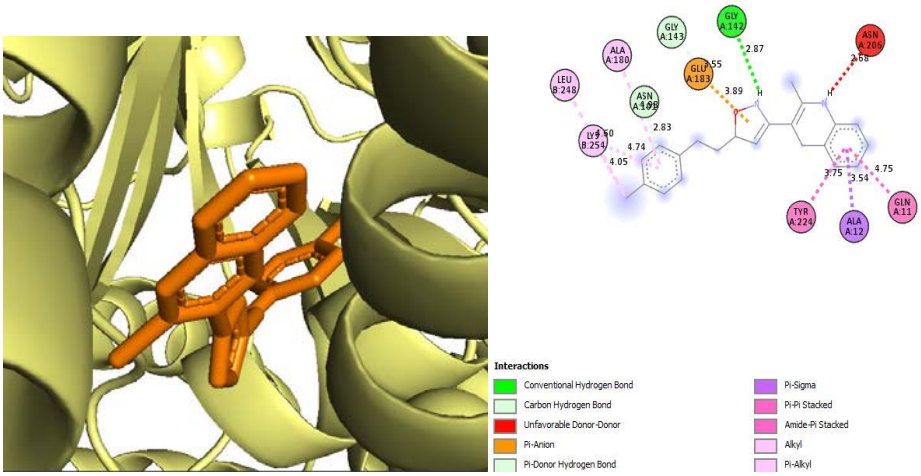

Figure 2. Best docking poses of the compound **7f** with colchicin.

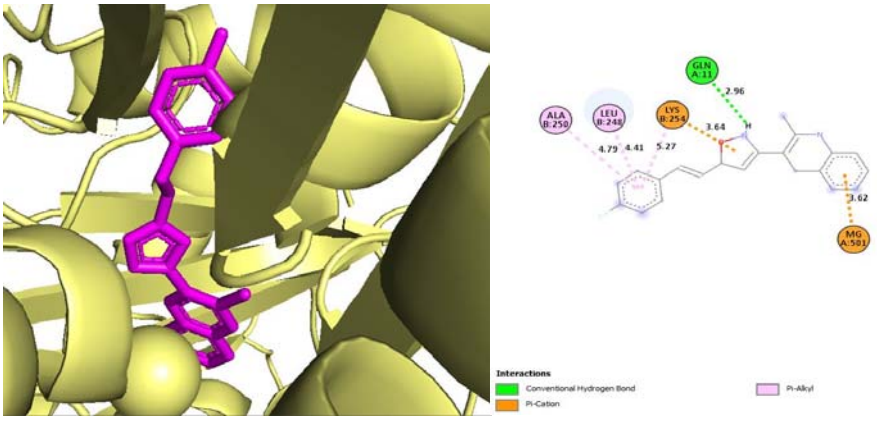

Figure 3. Best docking poses of the compound **7h** with colchicin.

5.4.1 ADMET study

ADME (Absorption, Distribution, Metabolism, Excretion) screening integrates pharmacokinetic properties and various drug-likeness parameters, including mutagenicity and toxicity, to evaluate the dosage levels of candidate compounds across different tissues. This process employs freely available online servers to examine and assess the ADME profiles of hit compounds identified through molecular docking. Given the significance of compounds interacting with enzymes, their potential as future drugs is being explored.[195] The ADME analysis of these molecules is detailed in Table **4** and **5**. For a compound to be considered eligible for use as a drug, the statistical results of the parameters obtained must meet specific standards. If the numerical values of the parameters fall outside these requirements, the compound is deemed unsuitable for drug use.[196] In drug discovery, the in-silico prediction of molecular physicochemical parameters, bioavailability, and pharmacokinetics is increasingly important for studying potential drug molecules efficiently. The ADME properties, which include the drug‘s access to the target and its elimination from the organism, are crucial in the early stages of drug discovery.[197] These parameters can be validated through in-silico studies utilizing computed physicochemical criteria were the first to propose a drug-likeness concept that examines.[198]

Drug-likeness is determined by several factors, including molar mass (≤500 gmol1), log P (≤5), number of hydrogen bond acceptors (≤10, based on N or O atoms in the molecule), and number of hydrogen bond donors (≤5, based on NH or OH groups in the molecule) and other rules such as Ghose[199] Veber[200] Egan[201] and Muegge[202] can also be utilized. The Swiss ADME web tool was employed for this purpose. The molecules being studied exhibit favourable ADME properties, adhering to Lipinski's rule of five principles, and have a bioavailability score of 0.55, indicating promising pharmacokinetic characteristics.[203] An acceptable range of molar refractivity was found in all cases. Compounds **5** and **7f** exhibited beneficial permeability values.[204] Similarly, the logarithmic values of S were determined to be **-6.91** and **-8.85** indicating poor solubility in the body **(Table 4 & 5**). Furthermore, the toxicity risk of compound **5** and **7a-l** was assessed using the ProTox-II web servers. The results indicated that both compounds fall under category IV, LD_{50} value of both the compounds was 800 mg/kg. In conclusion, compound **5**, **7f** and **7h** reveal promising characteristics that suggest their potential as pharmaceutical agents.

Table 4. Physicochemical and Pharmacokinetic properties of novel quinoline containing isoxazole derivatives **5** & **7a-l**.

Compound	MR	LogS	TPSA	iLOGP	WLOGP	GI absorption	BBB permeant	Pgp substrate	log Kp (cm/s)
5	75.09	-6.91	38.92	2.98	4.29	High	Yes	No	-5.54
7a	104.11	-8.36	48.15	3.89	5.5	High	Yes	No	-4.58
7b	102.59	-8.63	38.92	3.86	5.8	High	Yes	No	-4.21
7c	105.32	-9.04	38.92	3.99	6.26	High	No	No	-4.37
7d	104.11	-8.36	48.15	3.88	5.5	High	Yes	No	-4.58
7e	110.6	-8.46	57.38	4.04	5.51	High	Yes	No	-4.78
7f	102.63	-8.85	38.92	3.84	6.15	High	No	No	-4.15
7g	102.63	-8.85	38.92	3.65	6.15	High	No	No	-4.15
7h	97.58	-8.52	38.92	3.74	6.06	High	No	No	-4.41
7i	99.64	-7.67	59.15	3.1	5.2	High	Yes	No	-4.73
7j	115.13	-9.89	38.92	3.97	6.65	High	No	Yes	-3.79
7k	95.5	-7.52	67.16	3.54	5.56	High	No	No	-4.62
7l	109.48	-9.11	54.71	3.28	5.98	High	No	Yes	-4.53

Where, iLogP – liphophilicity; Log S – water solubility (SILICOS-IT; S-soluble, MS-moderately soluble); TPSA – topological polar surface area [Å2]; GI – gastrointestinalabsorption; BBB Permeant—Blood brain barrier; Pgp – p-glycoprotein inhibitors; Log Kp – skin permeability coefficient (Kp in cm/s).

Table 5. Drug-likeness properties of novel quinoline containing isoxazole derivatives **5** & **7a-l**.

Compound	MW	MLOGP	#H-bond acceptors	#H-bond donors	Lipinski #violations	Ghose #violations	Veber #violations	Egan #violations	Mugge #violations	Bioavailability Score
5	323.57	2.71	3	0	0	0	0	0	0	0.55
7a	362.81	3.34	4	0	0	0	0	0	1	0.55
7b	346.81	3.93	3	0	0	1	0	0	1	0.55
7c	411.68	4.3	3	0	1	1	0	1	1	0.55
7d	362.81	3.34	4	0	0	0	0	0	1	0.55
7e	392.83	3	5	0	0	0	0	0	1	0.55
7f	367.23	4.19	3	0	1	1	0	1	1	0.55
7g	367.23	4.19	3	0	1	1	0	1	1	0.55
7h	350.77	4.09	4	0	0	1	0	1	1	0.55
7i	348.78	3.12	4	1	0	0	0	0	1	0.55
7j	382.84	4.39	3	0	1	1	0	1	1	0.55
7k	338.81	3.29	3	0	0	0	0	0	1	0.55
7l	371.82	3.42	3	1	0	1	0	1	1	0.55

5.4.2 Molecular Dynamics Simulation analysis

The most favourable compounds after the docking analysis and ADMET Studies are compound **5** and **7f** in complex with the receptors 1ASO were further subjected to the molecular dynamic simulation study for a simulation time of 100 ns. The simulation study provided RMSD, RMSF, ligand torsion profile, ligand properties and protein-ligand contacts, Radius of Gyration (rGyr), Intra-molecular Hydrogen Bonds (intraHB), Molecular Surface Area (MolSA), Solvent Accessible Surface Area (SASA), and Polar Surface Area (PSA).[152]

The RMSD of atomic positions is used to calculate the average distance between the atoms of superimposed protein and ligand structures over time.[205] RMSD of proteins was illustrated in Figure **4a** and **5a**. When an MD simulation is balanced, RMSD analysis can show that oscillations near the simulation's end may be due to a thermal average structure. In RMSD, the average value of the cα-atoms in the compound **5**-1ASO complex after equilibrium was 2.62 Å. It has been observed that compound **5**-1ASO complexes have higher docking energies but are not stable during MDS analysis. On the other hand, the compound **7f**-1ASO complex shows more stability. Compound **7f**-1ASO complex showing very good stability up to 60 ns after that the fluctuation has been observed. This fluctuation is between ~1.0 Å, hence it is considered as a stable complex.

The RMSF is a parameter used to determine how and at what nanoseconds the protein fluctuated. It also explains how the ligand interacted with the protein and how much it fluctuated. Changes of 1-3 A° are acceptable for small and globular proteins. In our study we observed the average RMSF value of compound **5**-1ASO and **7f**-1ASO complexes were 0.89 A° (High 3.889 and low 0.361) and 1.36 A° (High 5.282 and low 0.457), respectively (**Figure 4b** & **5b**). Lower RMSF values in the system imply minor structural reorganizations and conformational changes at the binding site residues during the course of simulation. It suggests that the structure and organization of the protein do not deviate significantly from their original conformation after interacting with the compound. Further, In the context of ligand characteristics, we assessed various properties, including ligand RMSD, radius of gyration (rGyr), intramolecular hydrogen bonds (intraHB), molecular surface area (MolSA), solvent-accessible surface area (SASA), and polar surface area (PSA). Successful MDS demonstrate the stability of the compound **7f**-1ASO complex over time. This stability is essential for ensuring that the binding observed in molecular docking is not transient and that the complex can be maintained under physiological conditions.

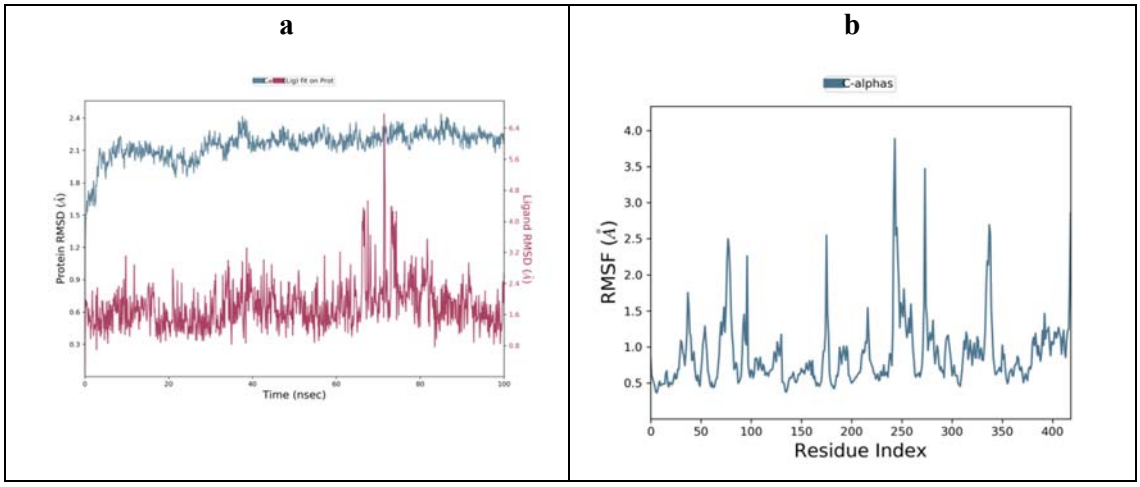

Figure 4. (**a**) RMSD trajectory plot of compound **5**-1ASO complexes, (**b**) RMSF trajectory plot of compound **5**-1ASO complexes.

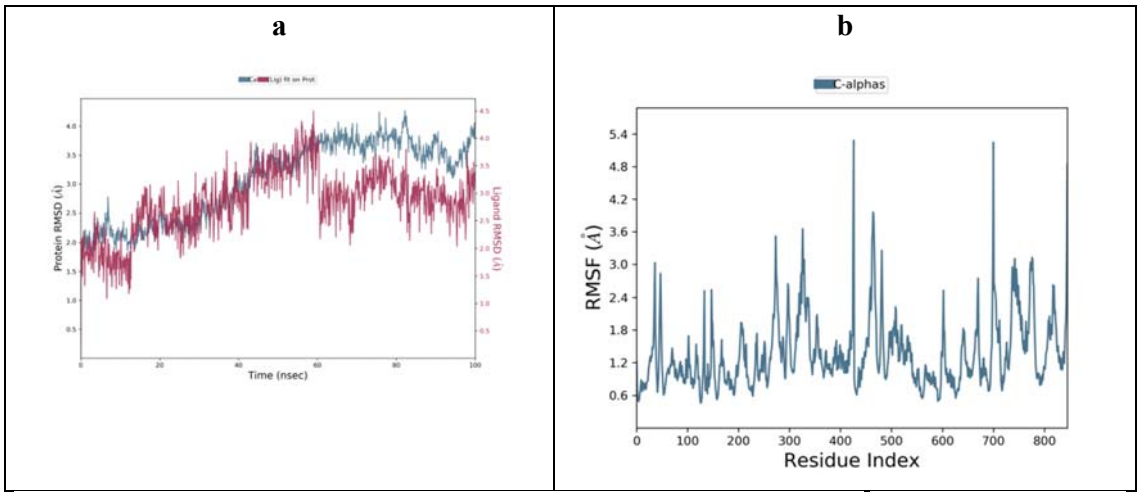

Figure 5. (**a**) RMSD trajectory plot of compound **7f**-1ASO complexes, (**b**) RMSF trajectory plot of compound **7f**-1ASO complexes.

5.4.3 Molecular mechanics and generalized born surface area (MM-GBSA) calculations

The MM-GBSA technique is widely used to determine the binding energy of ligands to protein molecules.[206] To enhance ligand ranking and predict binding energies more effectively, MMGBSA calculations were performed in compound **7a-l**. The calculated values represent

approximate binding free energies, where a more negative value signifies a stronger binding affinity and a stable configuration maintained throughout the simulation[207] and more negative binding energies were observed due to stable conformation of protein-ligand complex.[208,209] Hence, the entire findings from the simulation studies and MM-GBSA analysis indicate a noteworthy affinity of compound **7f** for the target 1ASO suggesting its potential as an inhibitor of the target protein. (**Table 6**).

Table 6. Binding free energy calculation of novel quinoline containing isoxazole derivatives compound **5** and **7f**.

Energies	Compound 5-1ASO (kcal/mol)	Compound 7f-1ASO (kcal/mol)
ΔG Bind[a]	-64.43	-88.22
ΔG Coulomb[b]	-6.69	-12.42
ΔG Hydrogen Bond[c]	-0.22	-0.56
ΔG Solvation[d]	11.36	16.60
ΔG Covalent[e]	0.73	1.56
ΔGLipo[f]	-30.63	-38.39
ΔGvdW[g]	-28.75	-52.07

Where, [a]ΔG Bind = Binding free energies, [b]ΔG Coulomb = Coulomb energy , [c]ΔG Hydrogen Bond = Hydrogen bond correction, [d]ΔG Solvation = Difference in free energy between a molecule in a solvent and in a gas phase, [e]ΔG Covalent = The amount of energy that is stored in the bond, [f]ΔGLipo = lipophilic energy, [g]ΔGvdW = Van der Waals interaction energy

5.4.4 Density functional theory (DFT) studies

Density Functional Theory (DFT) is a field focused on understanding the chemical reactivity and interactive behaviour of atoms and molecules. It provides a wide array of analytical tools to investigate the interactions within chemical systems.[210] Consequently, DFT plays a crucial

role in the field of drug design and discovery, particularly in virtual screening. DFT utilizes descriptors to provide insights into how drugs interact with receptors within the body. While it's important to note that these descriptors may not always directly correlate with the physiological chemistry of the human body, estimating CDFT descriptors can offer a qualitative understanding of these interactions. Electronegativity (χ) and global hardness (η) are chemical reactivity parameters that lack experimental counterparts. The electrophilicity index (ω) represents an equilibrium between an electrophile's inclination to gain more electron density and its hesitation to engage in the exchange of electron density with its environment.[211] In our study for compound **7f**, value of electronegativity was -0.31, global hardness was 0.03, global softness was 38.610, Chemical potential was -0.309, electrophilicity was 1.83, electro accepting power was 3.52 and Net electrophilicity was 3.54 (**Figure 6**)**.** By comprehending these features, chemists can make judicious decisions regarding the applicability of compound **7f** in diverse chemical, biological, or industrial contexts.

The ligand-protein contacts of compound **7f** show the specific residues of the protein that interact with the ligand (**Figure 7**). The ALA 12 forms several contacts with the ligand, suggesting its significant role in ligand binding. Whereas ASN 206 forms hydrogen bonds or ionic interactions with the ligand, indicated by the dashed lines connecting the nitrogen atom of ASN 206 to the ligand. The TYR 224 also forms an interaction with the ligand, likely contributing to the overall binding affinity. The protein-ligand contacts in the bar chart represent the interaction frequency of different residues with the ligand over a MDS (**Figure 8**). The different colours in the bars likely represent different types of interactions, such as hydrogen bonds, hydrophobic interactions, or electrostatic interactions. Overall, the varying interaction fractions suggest that certain residues like ASN 226 are consistently involved in ligand binding, while others may have more transient interactions.

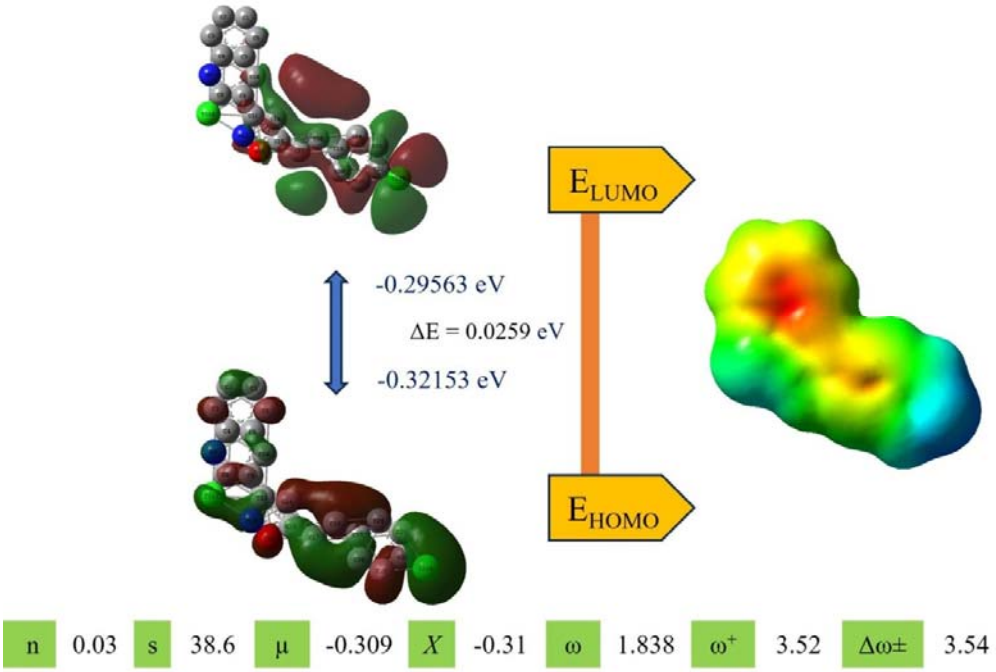

Figure 6. Frontier Molecular Orbitals (FMO) of compound **7f**.

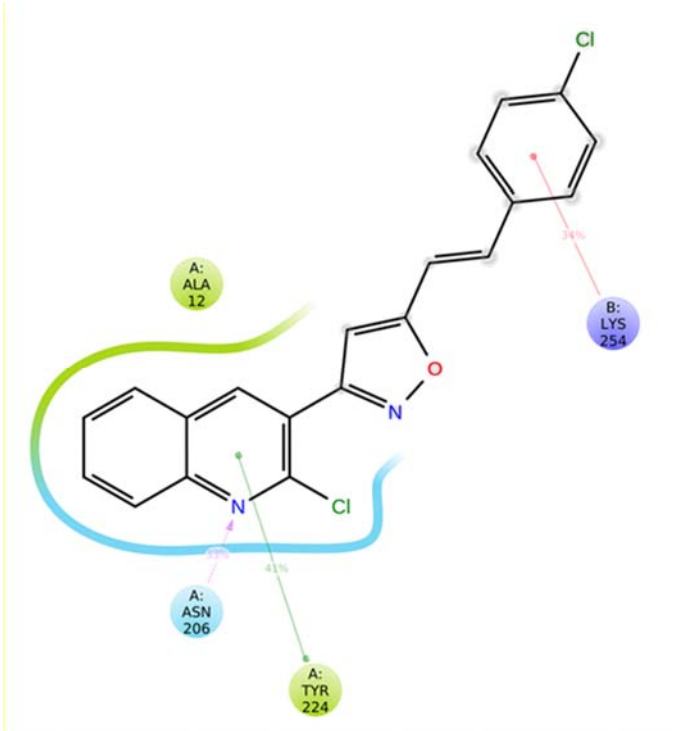

Figure 7. Interaction diagram of compound **7f**-protein contacts.

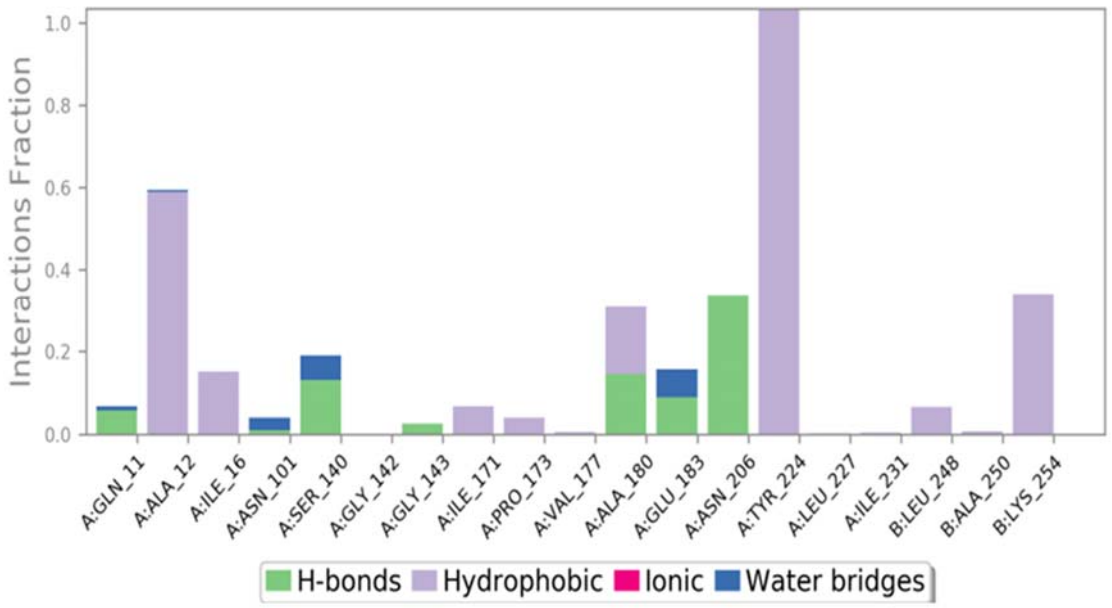

Figure 8. Interaction graph of protein-**7f** contacts.

5.5 Conclusion

A novel series of hybrid molecules of quinoline derivatives containing substituted isoxazole with Wittig reaction was synthesized and characterized using NMR and Mass spectral analysis. The synthesized compounds were evaluated for *in vitro* anticancer activity at the National Cancer Institute (NCI). The principal *in vitro* anticancer investigation was administering a single dose to all NCI 60 cell lines representing nine tumor subpanels: breast, CNS, ovarian, prostate, renal, colon, lung, melanoma, and leukemia. Following the demonstration of significant anti-cancer efficacy in preliminary screenings across all cell lines, three substances were selected for a five-dose assay. Out of all the synthesized compounds, three compounds **5, 7f** and **7h** showed promising results in cytotoxic activity with the highest docking score of -9.1 kJ/mol, -9.4 kJ/mol and -7.9 kJ/mol. Furthermore, docking and MD analysis revealed that compound **7f** may have exhibited anticancer potency through inhibition of tubulin-colchicine: stathmin-like domain complex (PDB:1SA0). As a part of docking study ADMET study, RMSD, RMSF, Molecular mechanics and generalized born surface area (MM-GBSA) calculations and Density functional theory (DFT) studies depicted. In that, compound **7f** for the target 1ASO suggesting its potential as an inhibitor of the target protein.

5.6 Experimental Section

5.6.1 Chemistry

The open-capillary method was used to determine all the melting points on an electrothermal device (SUNTEK), and the results are uncorrected. Compounds were detected in thin-layer chromatography with UV light at 254 nm, 365 nm and/or with iodine vapour on precoated silica gel 60 F254 (Merck). A Bruker AVANCE III (400 MHz) spectrometer was used to capture ^{1}H and ^{13}C NMR spectra in DMSO-d_6 and $CDCl_3$ using tetramethyl silane (TMS) as an internal standard, and chemical shifts are represented in ppm. Shimadzu GCMS QP2010 Ultra mass spectrometer was used to record mass spectra utilising a direct intake probe. All the reagents purchased from Sigma-Aldrich, Spectrochem and TCI and used without further purification.

Procedure for synthesis of ((3-(2-chloroquinolin-3-yl)isoxazol-5-yl)methyl)triphenyl-phosphonium bromide (6):

5-(Bromomethyl)-3-(2-chloroquinolin-3-yl)isoxazole (**5**, 200 mg, 0.62 mmol) in toluene, was added triphenylphosphine (195 mg, 0.74 mmol) and the mixture was stirred under reflux for 2 h. After completion of the reaction (monitored by TLC), the resultant precipitate was filtered and washed with toluene, then dried, which are sufficiently pure to use in the next step.

General procedure for the synthesis of compounds (7a-l):

((3-(2-chloroquinolin-3-yl)isoxazol-5-yl)methyl)triphenyl-phosphonium bromide (**6**, 1 mmol) and K_2CO_3 (2.5 mmol) were dissolved in DMSO and stirred at rt for the 30 minutes. After that, different substituted aryl aldehyde (1 mmol) was added and the reaction mixture was stirred at rt for 2 to 3 h. After the completion of the reaction (monitored by TLC), the reaction mixture was cooled to room temperature and poured onto crushed ice and precipitates was collected by filtration, washed with water, and dried. The obtained mass were washed with MeOH to give title compounds **(7a-l)**, which are analytically pure.

By using the same general synthetic procedure for **7a-l**, the following compounds were prepared:

(*E*)-3-(2-chloroquinolin-3-yl)-5-(4-methoxystyryl)isoxazole (7a):

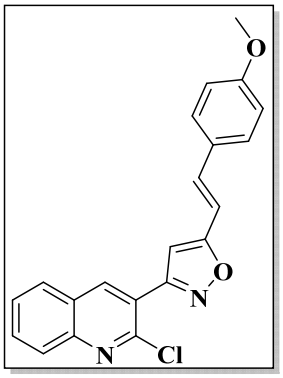

Compound **7a** was prepared from **6** (0.20 g, 0.41 mmol), 4-methoxy benzaldehyde (0.06 gm, 0.41 mmol) and K_2CO_3 (0.14 gm, 1.03 mmol) in DMSO. An off-white solid (0.19 g, 93% yield); mp: 203-205 °C. ^{1}H NMR (400 MHz, $CDCl_3$) δppm: 8.63 (s, 1H, Ar-H), 8.10 (d, *J* = 8.5 Hz, 1H, Ar-H), 7.93 (d, *J* = 8.0 Hz, 1H, Ar-H), 7.83 (t, *J* = 1.5 Hz, 1H, Ar-H), 7.66 (t, *J* = 8.2 Hz, 1H, Ar-H), 7.53 (d, *J* = 8.8 Hz, 2H, 2 × Ar-H), 7.42 (d, *J* = 16.4 Hz, 1H, CH), 6.98 – 6.91 (m, 3H, 2 × Ar-H, CH), 6.82 (s, 1H, Ar-H), 3.88 (s, 3H, OCH_3). ^{13}C NMR (101 MHz, $CDCl_3$) δppm: 168.89, 160.16, 159.68, 147.34, 139.26, 134.61, 131.11, 128.21, 127.94, 127.69, 127.62, 127.24, 126.29, 122.47, 113.92, 110.18, 101.61, 54.91. Mass spectrum: 363 *m/z* (M^+).

(*E*)-3-(2-chloroquinolin-3-yl)-5-(4-methylstyryl)isoxazole (7b):

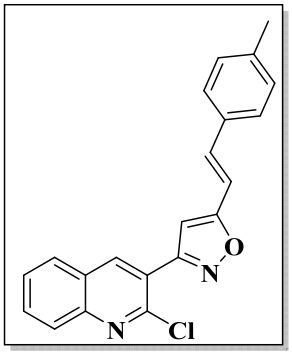

Compound **7b** was prepared from **6** (0.20 g, 0.41 mmol), 4-methyl benzaldehyde (0.05 gm, 0.41 mmol) and K_2CO_3 (gm, 1.03 mmol) in DMSO. An off-white solid (0.19 g, 97% yield); mp: 192-194 °C. ^{1}H NMR (400 MHz, DMSO) δppm: 8.84 (s, 1H, Ar-H), 8.18 (d, *J* = 8.1 Hz, 1H, Ar-H), 8.05 (d, *J* = 8.5 Hz, 1H, Ar-H), 7.93 (t, *J* = 7.8 Hz, 1H, Ar-H), 7.75 (t, *J* = 7.5 Hz, 1H, Ar-H), 7.61 (d, *J* = 7.7 Hz, 2H, 2 × Ar-H), 7.50 (d, *J* = 16.5 Hz, 1H, CH), 7.32 (d, *J* = 16.5 Hz, 1H, CH), 7.25 (d, *J* = 7.7 Hz, 2H, 2 × Ar-H), 7.14 (s, 1H, Ar-H), 2.34 (s, 3H, CH_3). ^{13}C NMR (101 MHz, DMSO) δppm: 169.53, 160.51, 147.57, 140.91, 139.61, 135.62, 133.03,

132.64, 130.01, 129.52, 129.11, 128.55, 128.18, 127.85, 126.91, 122.82, 112.59, 103.41, 21.45. Mass spectrum: 347 *m/z* (M^+).

(*E*)-5-(4-bromostyryl)-3-(2-chloroquinolin-3-yl)isoxazole (7c):

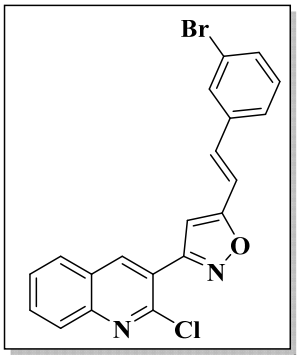

Compound **7c** was prepared from **6** (0.20 g, 0.41 mmol), 3-bromo benzaldehyde (0.08 gm, 0.41 mmol) and K_2CO_3 (gm, 0.62 mmol) in DMSO. An off-white solid (0.18 g, 90% yield); mp: 223-225 °C. ^{13}C NMR (101 MHz, DMSO) δppm: 168.93, 160.60, 147.58, 140.96, 135.12, 133.92, 132.68, 132.30, 131.76, 131.45, 131.09, 130.26, 129.12, 128.56, 128.17, 126.91, 122.85, 122.14, 115.17, 106.21, 104.40. Mass spectrum: 412 *m/z* (M^+).

(*E*)-3-(2-chloroquinolin-3-yl)-5-(3-methoxystyryl)isoxazole (7d):

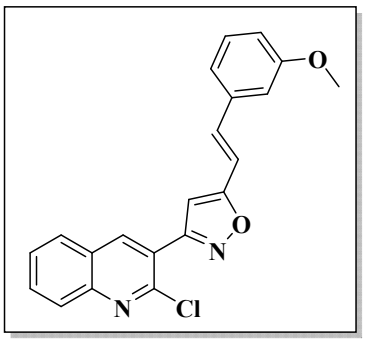

Compound **7d** was prepared from **6** (0.20 g, 0.41 mmol mmol), 3-methoxy benzaldehyde (0.06 gm, 0.41 mmol) and K_2CO_3 (gm, 1.03mmol) in DMSO. An off-white solid (0.19 g, 94% yield); mp: 202-204 °C. ^1H NMR (400 MHz, DMSO) δppm: 8.86 (s, 1H, Ar-H), 8.19 (d, J = 9.6 Hz, 1H, Ar-H), 8.06 (d, J = 8.4 Hz, 1H, Ar-H), 7.94 (t, J = 1.5 Hz, 1H, Ar-H), 7.76 (t, J = 1.3 Hz, 1H, Ar-H), 7.55 – 7.30 (m, 5H, 3 × Ar-H, 2 × CH), 7.18 (s, 1H, Ar-H), 6.97 (d, J = 8.1 Hz, 1H), 3.82 (s, 3H, OCH_3). ^{13}C NMR (101 MHz, DMSO) δppm: 169.32, 160.55, 160.14, 147.78, 147.58, 140.93, 137.20, 135.58, 132.66, 130.42, 129.11, 128.55, 128.18, 126.91, 122.77, 120.55, 115.85, 113.91, 112.62, 103.82, 55.68. Mass spectrum: 363 *m/z* (M^+).

(*E*)-3-(2-chloroquinolin-3-yl)-5-(3,4-dimethoxystyryl)isoxazole (7e):

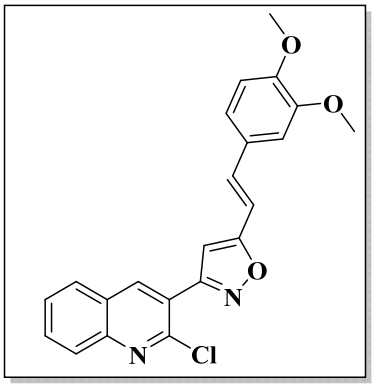

Compound **7e** was prepared from **6** (0.20 g, 0.41 mmol mmol), 3,4-dimethoxy benzaldehyde (0.07 gm, 0.41 mmol) and K_2CO_3 (gm, 0.62 mmol) in DMSO. An off-white solid (0.17 g, 84% yield); mp: 206-208 °C. ^{1}H NMR (400 MHz, DMSO) δppm: 8.86 (s, 1H, Ar-H), 8.19 (d, *J* = 8.1 Hz, 1H, Ar-H), 8.06 (d, *J* = 8.4 Hz, 1H, Ar-H), 7.94 (t, *J* = 7.7 Hz, 1H, Ar-H), 7.76 (t, *J* = 7.5 Hz, 1H, Ar-H), 7.48 (d, *J* = 16.5 Hz, 1H, CH), 7.38 (s, 1H, Ar-H), 7.31 (d, *J* = 16.5 Hz, 1H, CH), 7.23 (d, *J* = 8.3, 2.0 Hz, 1H, Ar-H), 7.10 (s, 1H, Ar-H), 7.01 (d, *J* = 8.3 Hz, 1H, Ar-H), 3.83 (d, *J* = 15.8 Hz, 6H, 2 × OCH_3). ^{13}C NMR (101 MHz, DMSO) δppm: 169.81, 160.47, 150.59, 149.51, 147.81, 147.56, 140.88, 135.80, 132.63, 129.10, 128.63, 128.54, 128.18, 126.92, 122.88, 122.13, 112.14, 111.38, 110.06, 102.84, 56.04. Mass spectrum: 393 *m/z* (M^+).

(*E*)-3-(2-chloroquinolin-3-yl)-5-(4-chlorostyryl)isoxazole (7f):

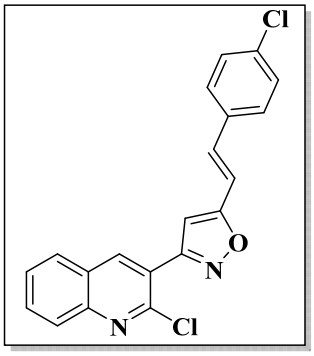

Compound **7f** was prepared from **6** (0.20 g, 0.41 mmol mmol), 4-chloro benzaldehyde (0.06 gm, 0.41 mmol) and K_2CO_3 (gm, 0.62 mmol) in DMSO. An off-white solid (0.18 g, 92% yield); mp: 218-220 °C. ^{1}H NMR (400 MHz, DMSO) δppm: 8.87 (s, 1H, Ar-H), 8.19 (d, *J* = 8.2 Hz, 1H, Ar-H), 8.06 (d, *J* = 8.4 Hz, 1H, Ar-H), 7.94 (t, *J* = 7.6 Hz, 1H, Ar-H), 7.80 – 7.71 (m, 3H, 3 × Ar-H), 7.60 – 7.48 (m, 3H, 2 × Ar-H, CH), 7.44 (d, *J* = 16.6 Hz, 1H, CH), 7.20 (s, 1H, Ar-

H). ^{13}C NMR (101 MHz, DMSO) δppm: 169.12, 160.59, 147.77, 147.59, 140.96, 134.77, 134.27, 132.69, 130.98, 129.58, 129.44, 129.12, 128.57, 128.19, 126.92, 122.72, 114.37, 104.09. Mass spectrum: 367 *m/z* (M^+).

(*E*)-3-(2-chloroquinolin-3-yl)-5-(2-chlorostyryl)isoxazole (7g):

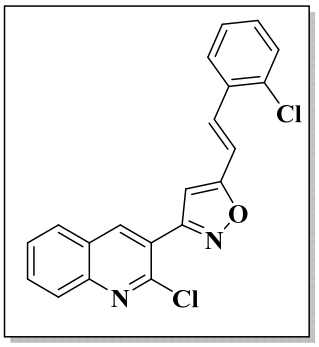

Compound **7g** was prepared from **6** (0.20 g, 0.41 mmol mmol), 2-chloro benzaldehyde (0.06 gm, 0.41 mmol) and K_2CO_3 (gm, 0.62 mmol) in DMSO. An off-white solid (0.18 g, 90% yield); mp: 215-217 °C. ^{1}H NMR (400 MHz, DMSO) δppm: 8.78 (s, 1H, Ar-H), 8.14 (d, *J* = 8.1 Hz, 1H, Ar-H), 8.01 (d, *J* = 8.7 Hz, 1H, Ar-H), 7.91 (t, *J* = 8.1 Hz, 1H, Ar-H), 7.73 (t, *J* = 7.7 Hz, 1H, Ar-H), 7.58 (d, *J* = 7.9 Hz, 1H, Ar-H), 7.50 (d, *J* = 8.0 Hz, 1H, Ar-H), 7.43 (q, *J* = 8.0, 7.4 Hz, 2H, 2 × Ar-H), 7.09 (d, *J* = 16..6 Hz, 1H, CH), 6.92 (d, *J* = 16.6 Hz, 1H, CH), 6.72 (s, 1H, Ar-H). Mass spectrum: 367 *m/z* (M^+).

(*E*)-3-(2-chloroquinolin-3-yl)-5-(4-fluorostyryl)isoxazole (7h):

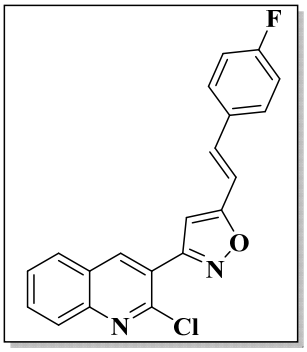

Compound **7h** was prepared from **6** (0.20 g, 0.41 mmol mmol), 4-fluro benzaldehyde (0.05 gm, 0.41 mmol) and K_2CO_3 (gm, 0.62 mmol) in DMSO. An off-white solid (0.18 g, 88% yield); mp: 209-211 °C. ^{1}H NMR (400 MHz, DMSO) δppm: 8.86 (s, 1H), 8.19 (d, *J* = 8.6 Hz, 1H), 8.06 (d, *J* = 9.0 Hz, 1H), 7.94 (s, 1H), 7.83 – 7.74 (m, 3H), 7.56 (d, *J* = 15.6 Hz, 1H), 7.37 (d, *J* = 16.4 Hz, 1H), 7.30 (t, *J* = 8.7 Hz, 2H), 7.17 (s, 1H). ^{13}C NMR (101 MHz, DMSO) δppm:

169.29, 160.56, 147.77, 147.57, 140.94, 134.45, 132.67, 132.44, 130.09, 130.01, 129.12, 128.56, 128.18, 126.91, 122.76, 116.50, 116.29, 113.49, 103.73. Mass spectrum: 351 *m/z* (M^+).

(*E*)-2-(2-(3-(2-chloroquinolin-3-yl)isoxazol-5-yl)vinyl)phenol (7i):

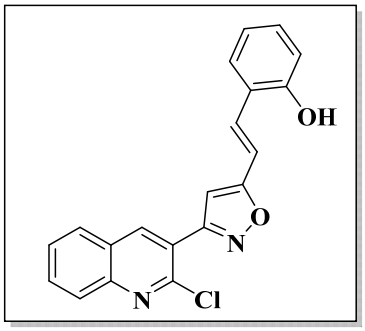

Compound **7i** was prepared from **6** (0.20 g, 0.41 mmol mmol), 2-hydroxy benzaldehyde (0.05 gm, 0.41 mmol) and K_2CO_3 (gm, 1.03 mmol) in DMSO. An off-white solid (0.17 g, 96% yield); mp: 196-198 °C. ^{1}H NMR (400 MHz, DMSO) δppm: 10.21 (s, 1H, Ar-OH), 8.84 (s, 1H, Ar-H), 8.17 (d, *J* = 8.1 Hz, 1H, Ar-H), 8.04 (d, *J* = 8.4 Hz, 1H, Ar-H), 7.92 (t, *J* = 7.8 Hz, 1H, Ar-H), 7.73 (d, *J* = 15.4, 7.8 Hz, 1H, CH), 7.66-7.63 (m, 2H, 2 × Ar-H), 7.38 (d, *J* = 16.8 Hz, 1H, CH), 7.21 (t, *J* = 7.8 Hz, 1H, Ar-H), 7.13 (s, 1H, Ar-H), 6.94 (d, *J* = 8.1 Hz, 1H, Ar-H), 6.87 (d, *J* = 7.6 Hz, 1H, Ar-H). ^{13}C NMR (101 MHz, DMSO) δppm: 169.91, 160.51, 156.60, 147.81, 147.54, 140.88, 132.59, 131.33, 130.96, 129.08, 128.50, 128.17, 126.90, 122.88, 122.39, 119.92, 116.58, 113.05, 103.14. Mass spectrum: 349 *m/z* (M^+).

(*E*)-3-(2-chloroquinolin-3-yl)-5-(2-(naphthalen-1-yl)vinyl)isoxazole (7j):

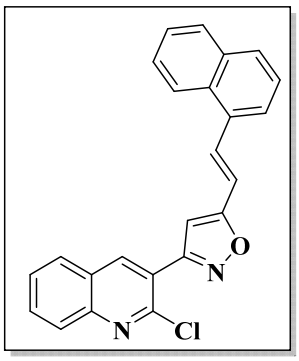

Compound **7j** was prepared from **6** (0.20 g, 0.41 mmol mmol), 1-naphthaldehyde (0.41 mmol) and K_2CO_3 (0.06 gm, 1.03 mmol) in DMSO. An off-white solid (0.16 g, 80% yield); mp: 205-207 °C. ^{1}H NMR (400 MHz, DMSO) δppm: 8.88 (s, 1H, Ar-H), 8.43 (d, *J* = 8.3 Hz, 1H, Ar-H), 8.39 (d, *J* = 16.3 Hz, 1H, Ar-H), 8.20 (d, *J* = 8.0 Hz, 1H, Ar-H), 8.13 – 7.84 (m, 5H, 5 ×

Ar-H), 7.81 – 7.73 (m, 2H, 2 × Ar-H), 7.66 – 7.52 (m, 2H, 2 × Ar-H), 7.48 (d, *J* = 16.3 Hz, 1H, CH), 7.43 (s, 1H, Ar-H). ^{13}C NMR (101 MHz, DMSO) δppm: 169.66, 160.59, 147.60, 140.95, 140.70, 137.29, 135.49, 133.87, 132.67, 130.10, 129.13, 128.57, 128.20, 128.10, 127.32, 126.73, 126.27, 126.01, 124.64, 123.94, 122.83, 117.43, 116.06, 103.89. Mass spectrum: 383 *m/z* (M^+).

(*E*)-3-(2-chloroquinolin-3-yl)-5-(2-(thiophen-2-yl)vinyl)isoxazole (7k):

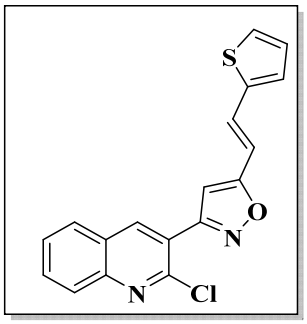

Compound **7k** was prepared from **6** (0.20 g, 0.41 mmol mmol), thiophene-2-carbaldehyde (0.05 mmol) and K_2CO_3 (gm, 1.03 mmol) in DMSO. An off-white solid (0.17 g, 96% yield); mp: 190-192 °C. ^{1}H NMR (400 MHz, DMSO) δppm: 8.84 (s, 1H), 8.18 (d, *J* = 8.2 Hz, 1H), 8.05 (d, *J* = 8.4 Hz, 1H), 7.93 (t, *J* = 7.7 Hz, 1H), 7.79 – 7.64 (m, 3H), 7.47 (d, *J* = 3.6 Hz, 1H), 7.23 – 7.12 (m, 2H), 7.07 (d, *J* = 16.3 Hz, 1H). ^{13}C NMR (101 MHz, DMSO) δppm: 168.84, 160.51, 147.74, 147.57, 140.89, 140.76, 132.64, 130.29, 130.06, 129.11, 128.91, 128.64, 128.53, 128.17, 126.90, 122.73, 112.19, 103.70. Mass spectrum: 339 *m/z* (M^+).

(*E*)-5-(4-bromostyryl)-3-(2-chloroquinolin-3-yl)isoxazole (7l):

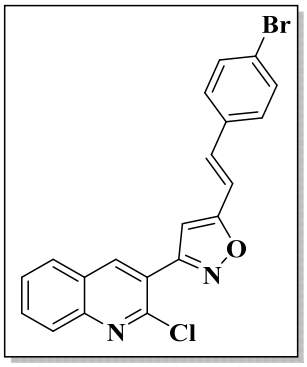

Compound **7l** was prepared from **6** (0.20 g, 0.41 mmol mmol), 4-bromo benzaldehyde (0.06 gm, 0.41 mmol) and K_2CO_3 (gm, 1.03 mmol) in DMSO. An off-white solid (0.17 g, 96% yield); mp: 225-227 °C. ^{1}H NMR (400 MHz, DMSO) δppm: 8.86 (s, 1H), 8.19 (d, *J* = 8.3 Hz, 1H), 8.06 (d, *J* = 8.4 Hz, 1H), 7.94 (t, *J* = 7.7 Hz, 1H), 7.76 (dt, *J* = 7.2, 3.4 Hz, 3H), 7.60 – 7.48 (m,

3H), 7.44 (d, *J* = 16.5 Hz, 1H), 7.19 (s, 1H).^{13}C NMR (101 MHz, DMSO) δppm: 169.11, 160.58, 147.76, 147.59, 140.94, 134.77, 134.27, 134.23, 132.67, 130.97, 129.57, 129.43, 129.12, 128.98, 128.56, 128.18, 126.91, 122.72, 114.37, 104.08. Mass spectrum: 412 *m/z* (M^+).

5.6.2 protein and ligand preparation for molecular docking:

In this work, the binding of newly synthesized compounds to tubulin-colchicine: stathmin-like domain complex was investigated using a computer-based docking approach. The X-ray crystal structure of the target tubulin-colchicine: stathmin-like domain complex (PDB:1SA0) was retrieved from the RCSB Protein Data Bank web server (www.rcsb.org/pdb/).[212] The two-dimensional chemical structures of the synthetic compounds are drawn using ChemDrawUltra 0.7, and then converted to SDF format using Open Babel 2.4.1 tool.[213] The docking area is selected by generating a grid box centred at x, y and z coordinates. The in silico docking study between the synthetic compounds and the binding site pocket of the target is carried out using a PyRx 8.0 tool. The binding poses were clustered and ranked in the order of their binding affinities. The molecular interactions (hydrogen bonds and hydrophobic interactions) between the target proteins and compounds were studied using LigPlot + version 2.2.8.[214]

5.6.3 In-silico ADMET Study

The concept of drug-like chemical species is extensively used in drug discovery and the selection of potential candidates. Compounds with pharmacokinetic properties that allow them to persist through human-phase clinical trials are considered to be drug-like.[215] To assess the physicochemical properties, pharmacokinetic profile, drug similarity, and medicinal chemistry of these compounds, the SwissADME was utilized.[216] This evaluation included analyzing their lipophilicity and water solubility.[217] The 2D structures from the database were converted into a string-based search format, enabling efficient screening and analysis of potential drug candidates. To estimate toxicity risk, the web server PROTOX II was utilised.[218]

5.6.4 Molecular Dynamics Simulation Studies and MM-GBSA calculations

Schrödinger LLC Desmond software that was used for molecular dynamics for 100 nanoseconds.[219] Prior to MD simulation, docking of protein and ligand was carried out as a first crucial step that predicted a static view of molecule's binding position at the protein's active site. By incorporating Newton's classical equation of motion, MD simulations generally simulate atom movements throughout the time and predict ligand-binding status in

physiological environment. The ligand-receptor complex was pre-processed by Maestro's Protein Preparation Wizard which included optimization, minimization and fill missing residues if needed as well as the system created via System Builder tool. TIP3P solvent model was used that based on an orthorhombic box with 300 K temperature, 1 atm pressure and OPLS_2005 force field. Using counter ions and 0.15 M sodium chloride, the models were neutralized and to simulate physiological conditions respectively. Models were loosened before simulation and trajectories were stored for inspection after every 100 ps.

The molecular mechanics generalized Born surface area (MM-GBSA) module of prime was used to determine the binding free energy (Gbind) of docked complex during MD simulations of final complexes. Using the OPLS 2005 force field, VSGB solvent model and rotamer search techniques, the binding free energy was estimated. The MD trajectory frames were chosen at intervals of 100 ns after the MD run. The total free energy binding was calculated using following equation:

dGbind = Gcomplex- (Gprotein + Gligand)

Where, dGbind = binding free energy, Gcomplex = free energy of the complex,

Gprotein = free energy of the target protein, Gligand = free energy of the ligand.

5.6.5 Density functional theory (DFT) studies

Hence, the aim of this approach is to offer comprehensive geometric information for a broad spectrum of systems. The theoretical computations were performed using the DFT method with the B3LYP-6-311G basis set.[220] To conduct important chemical calculations, including the generation of molecular electrostatic potential surfaces, HOMO and LUMO surfaces, as well as global reactivity parameters, the input files for the intended molecules were prepared and organised using the Gauss-view 06 software.[221]

5.7 Spectral data

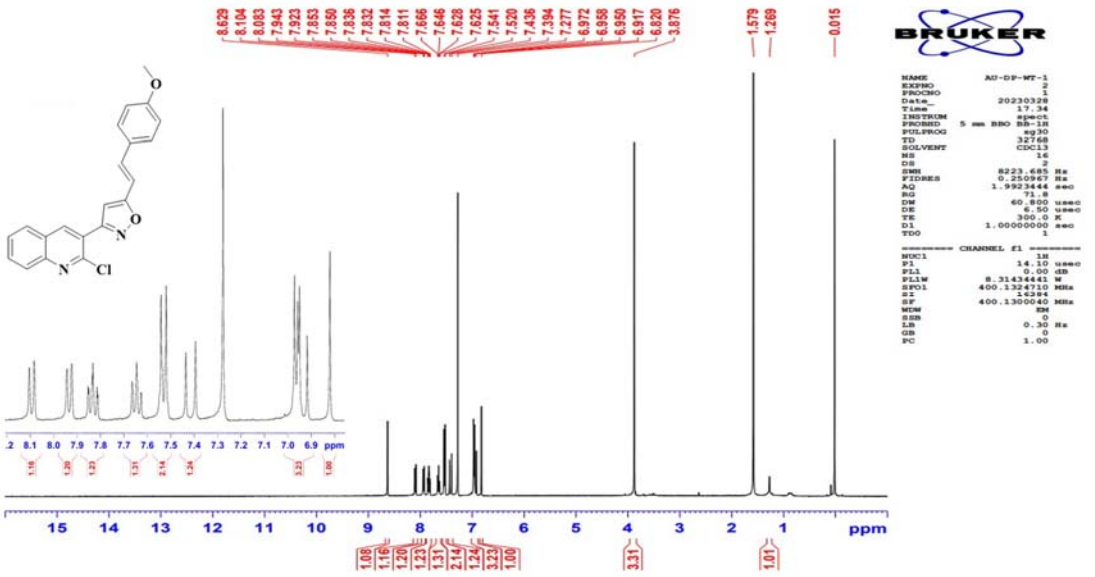

Figure 1: ^{1}H NMR spectra of compound **7a**

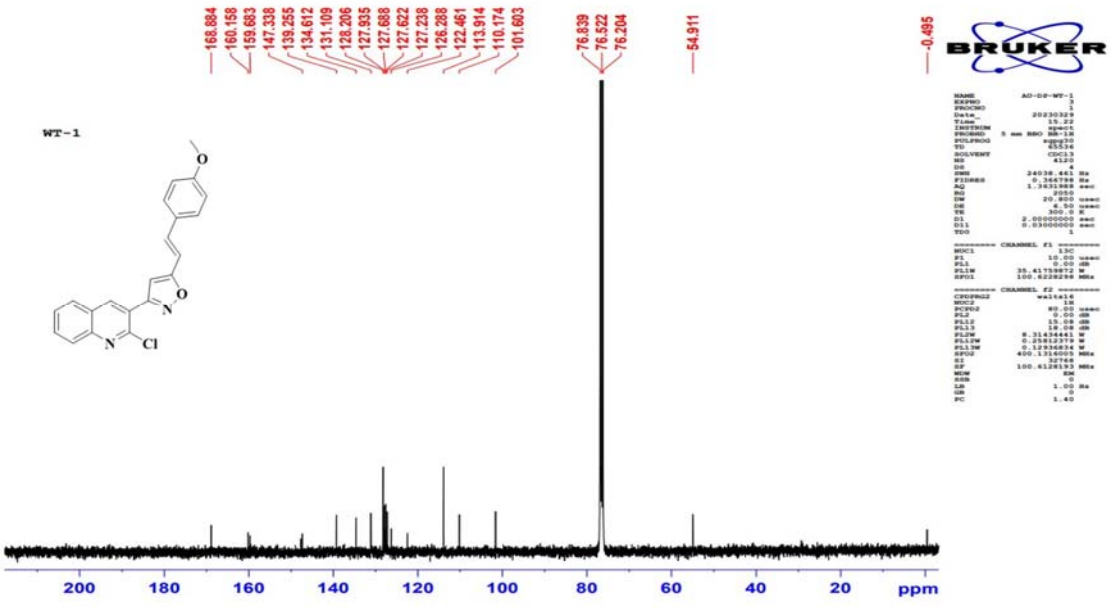

Figure 2: ^{13}C NMR spectra of compound **7a**

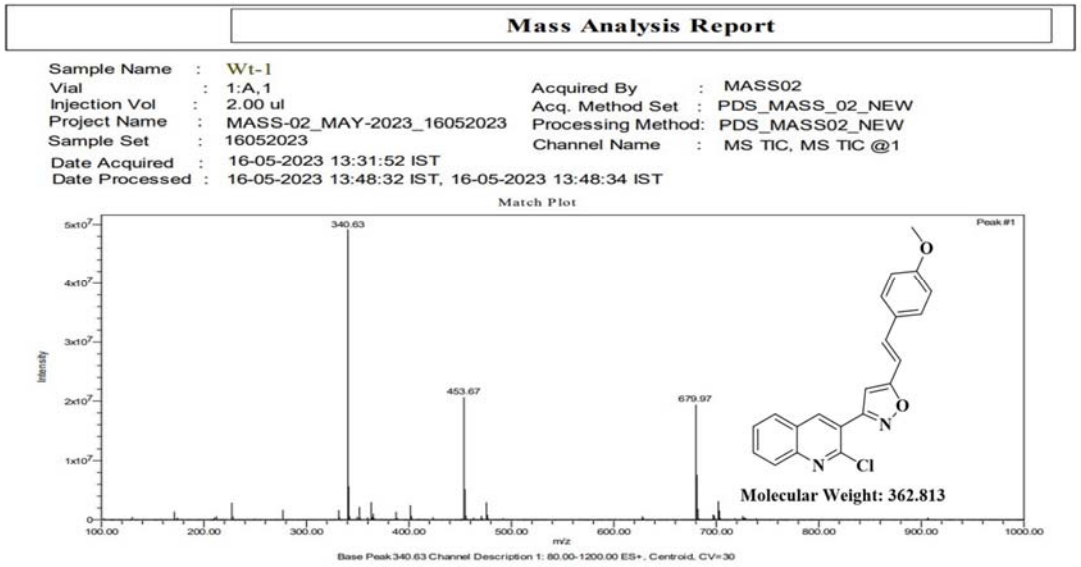

Figure 3: Mass spectra of compound **7a**

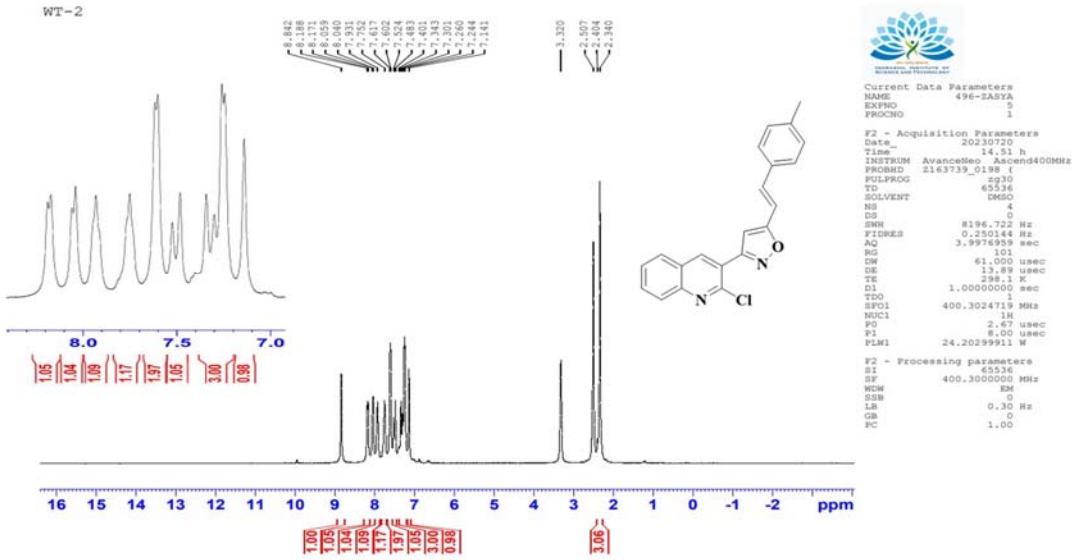

Figure 4: ^{1}H NMR spectra of compound **7b**

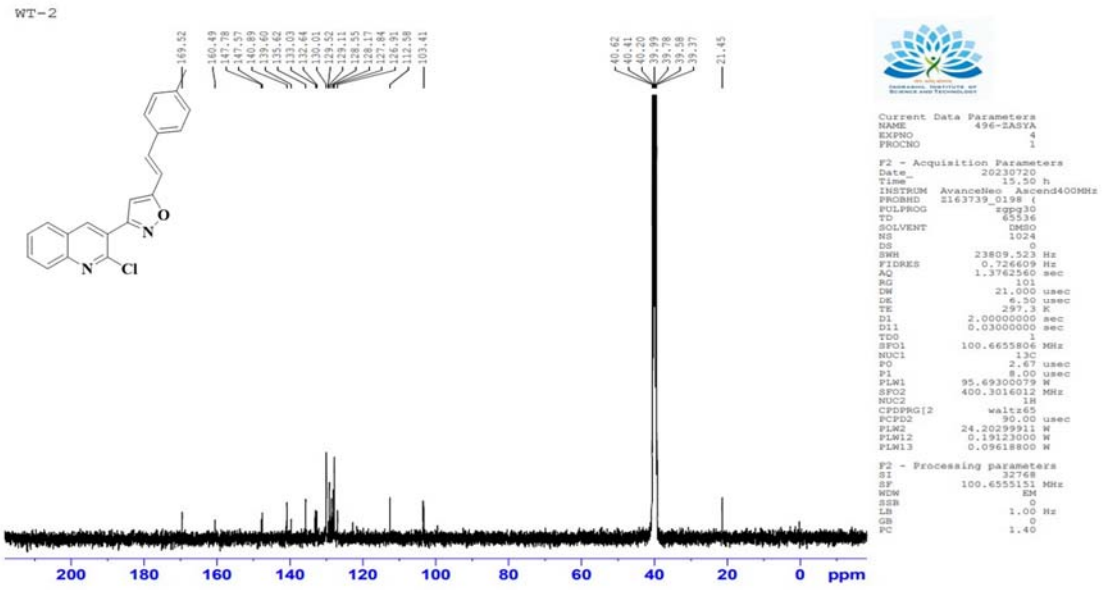

Figure 5: ^{13}C NMR spectra of compound **7b**

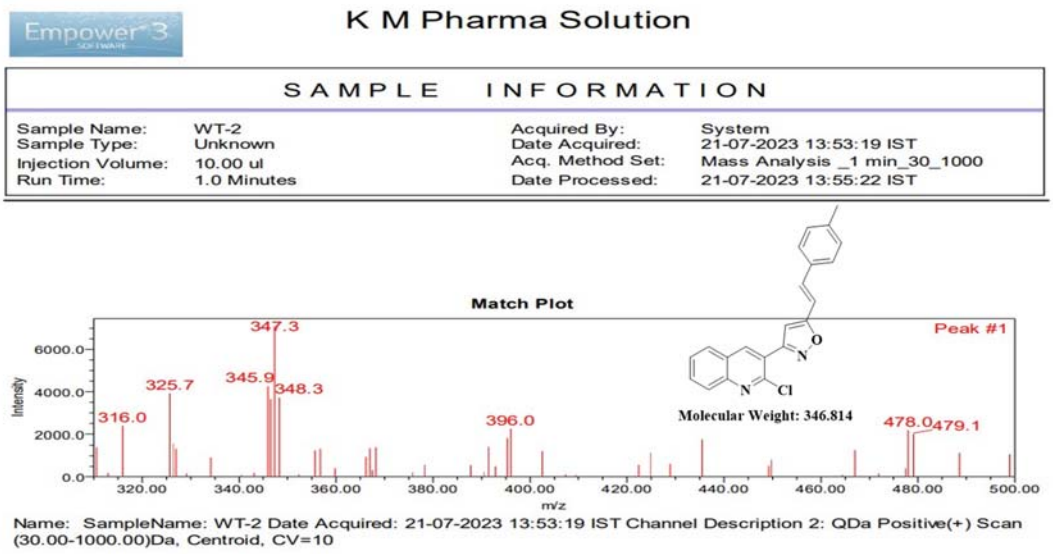

Figure 6: Mass spectra of compound **7b**

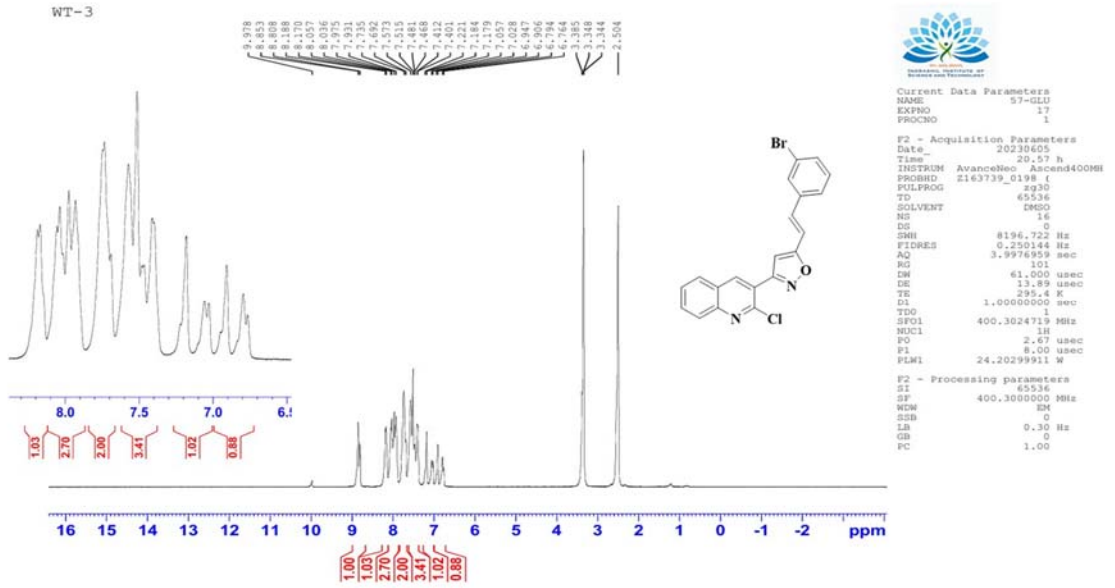

Figure 7: ^{1}H NMR spectra of compound **7c**

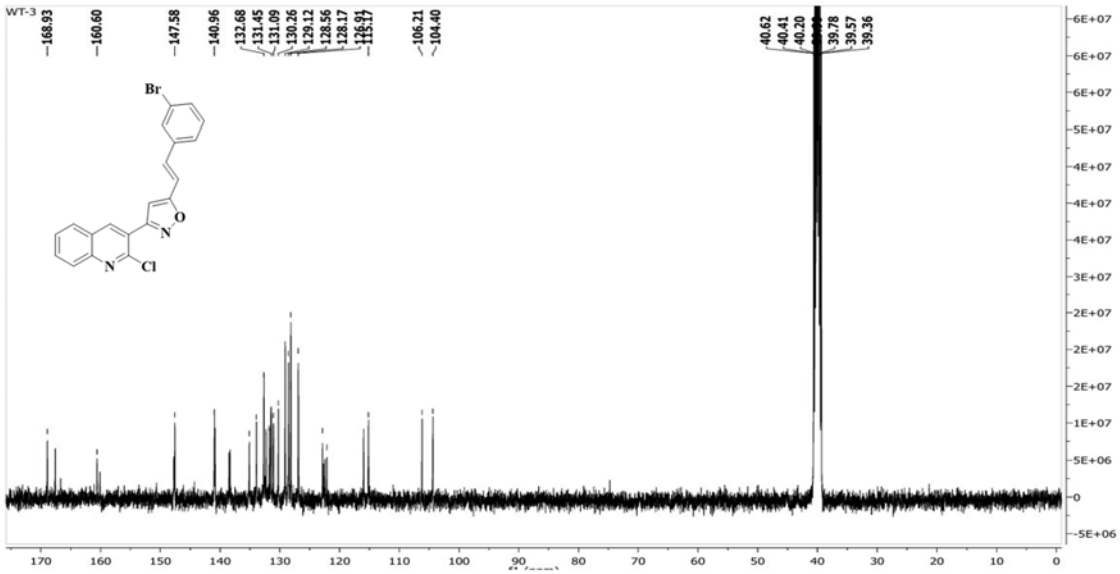

Figure 8: ^{13}C NMR spectra of compound **7c**

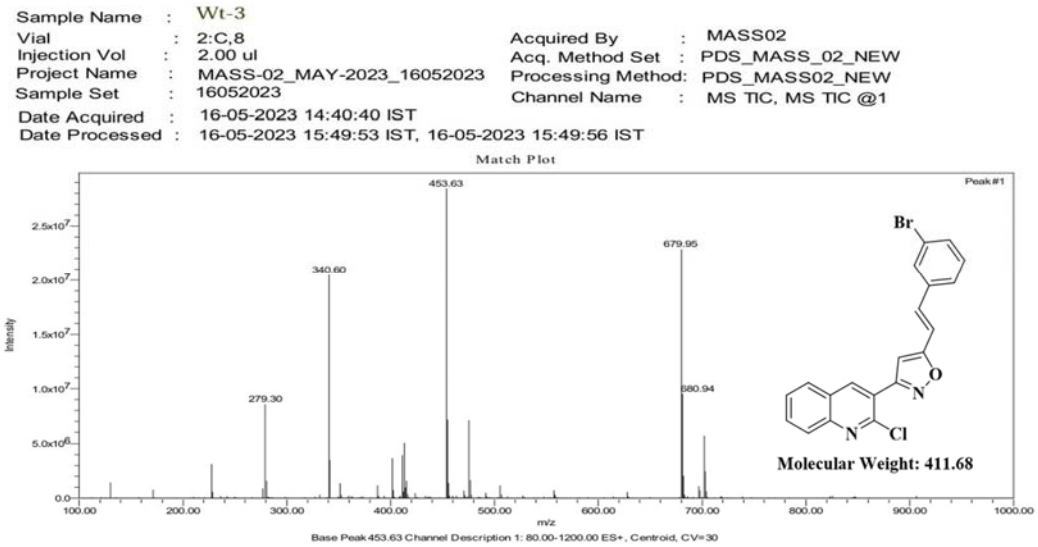

Figure 9: Mass spectra of compound **7c**

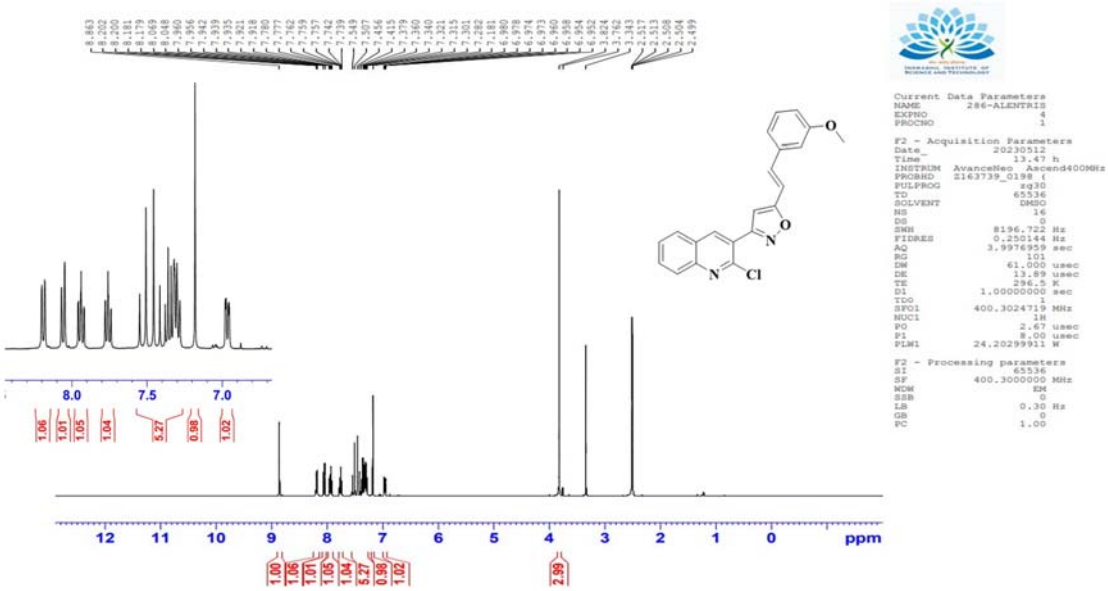

Figure 10: ^{1}H NMR spectra of compound **7d**

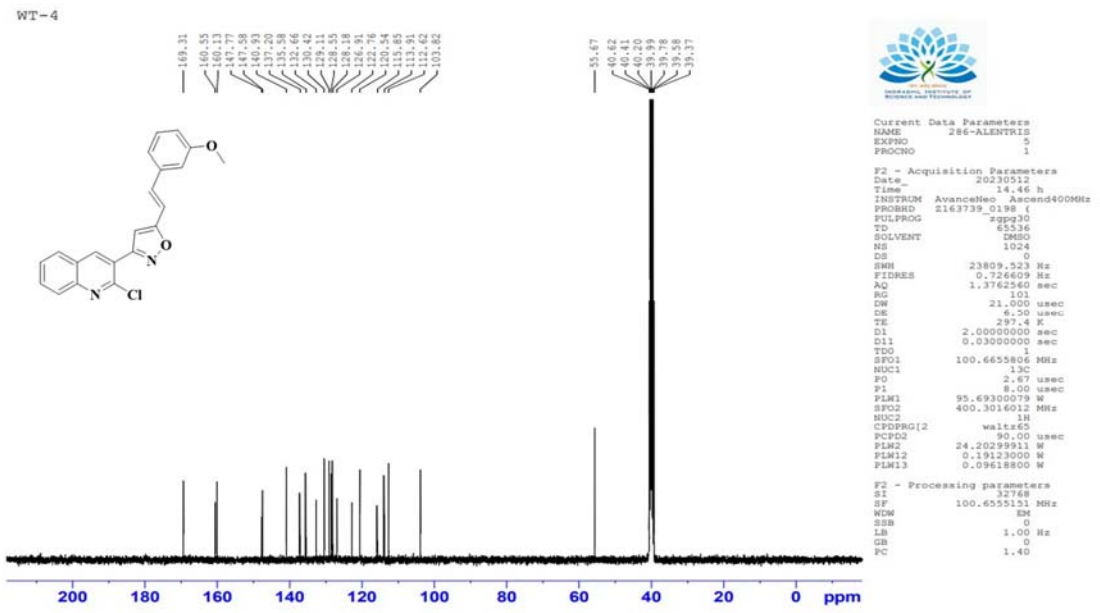

Figure 11: ^{13}C NMR spectra of compound **7d**

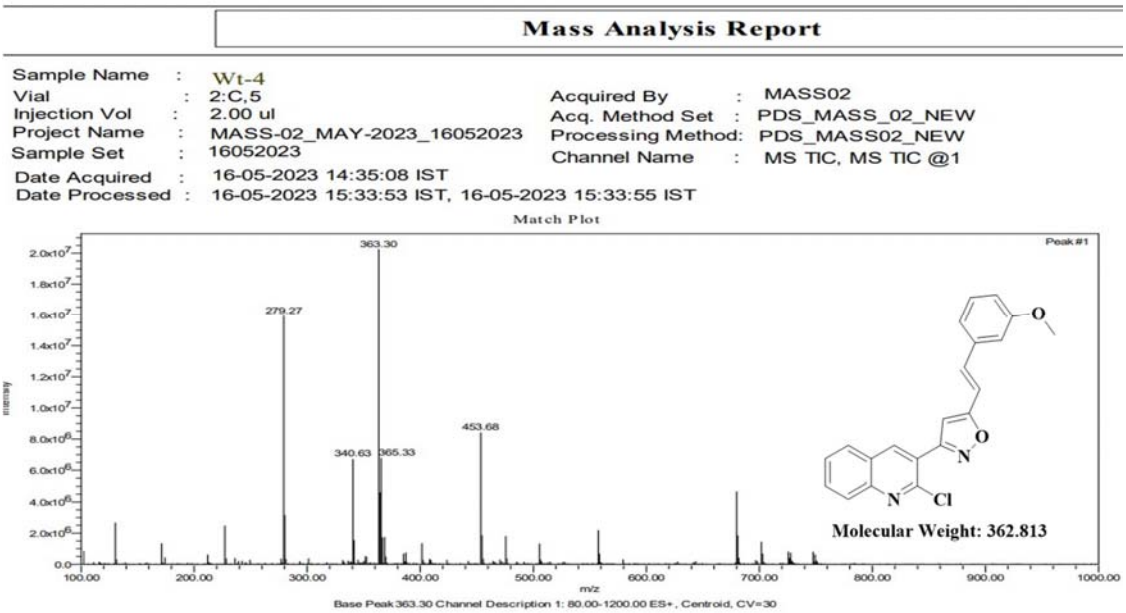

Figure 12: Mass spectra of compound **7d**

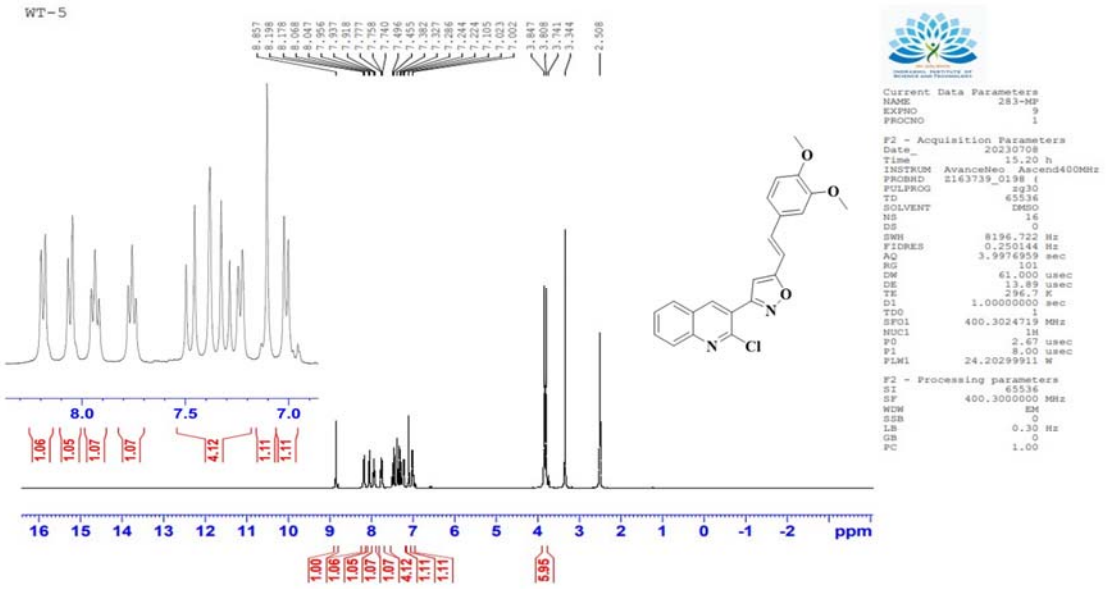

Figure 13: ^{1}H NMR spectra of compound **7e**

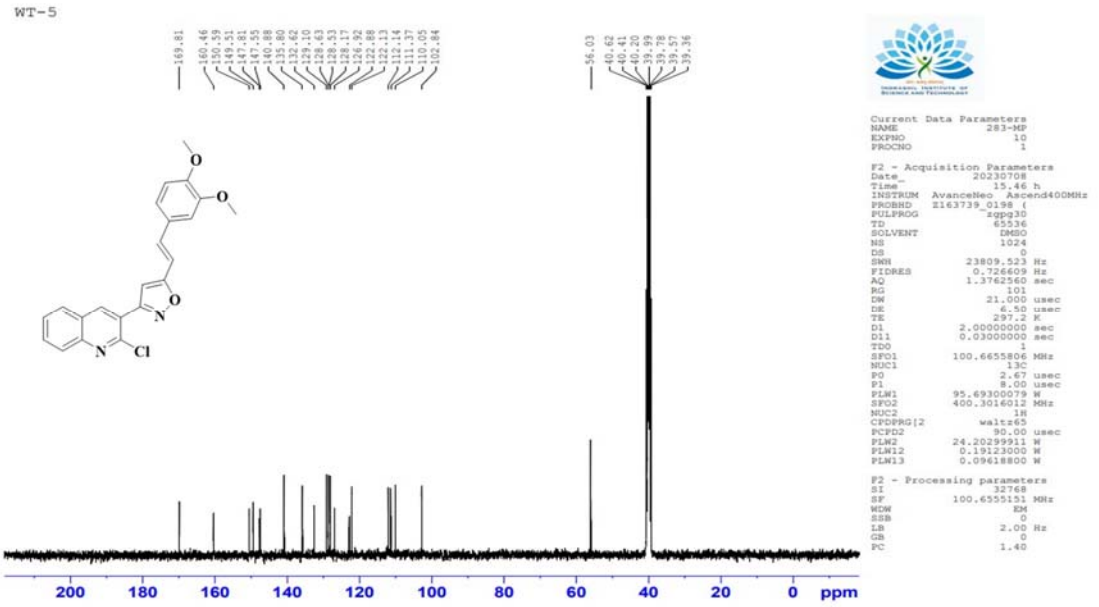

Figure 14: ^{13}C NMR spectra of compound **7e**

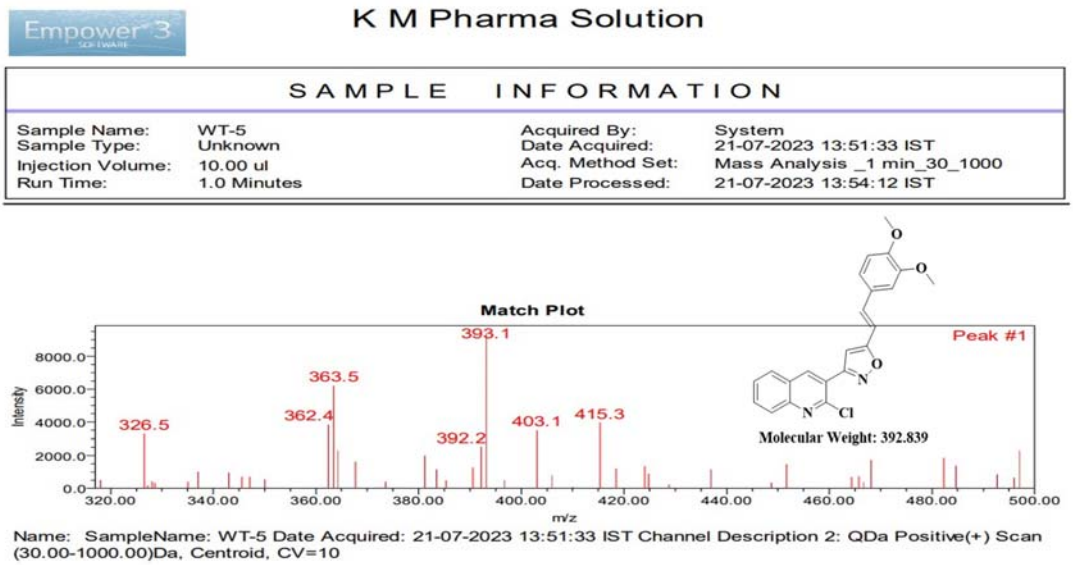

Figure 15: Mass spectra of compound **7e**

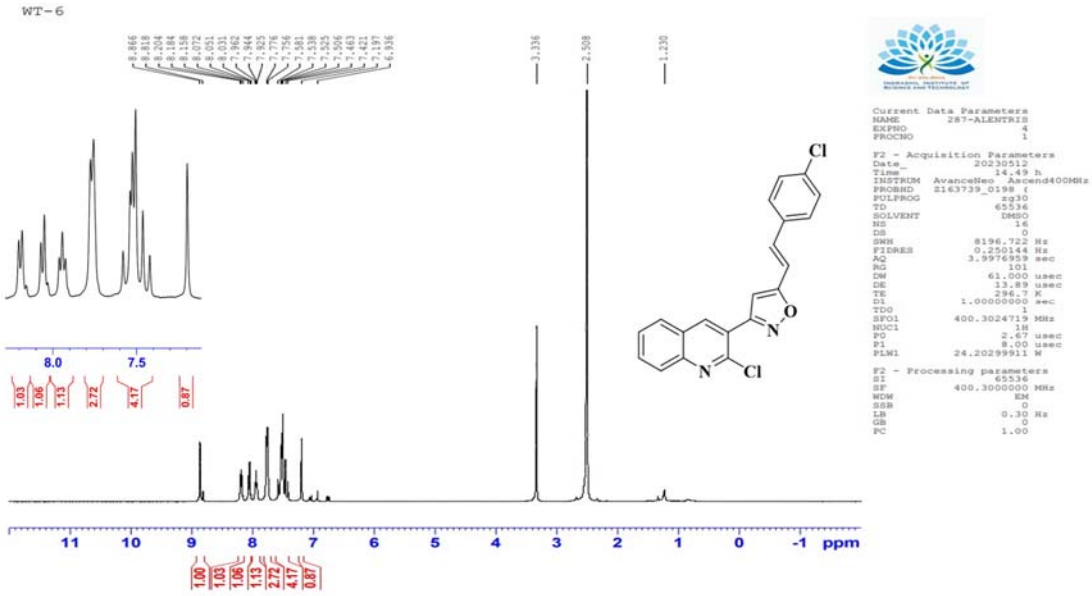

Figure 16: ^{1}H NMR spectra of compound **7f**

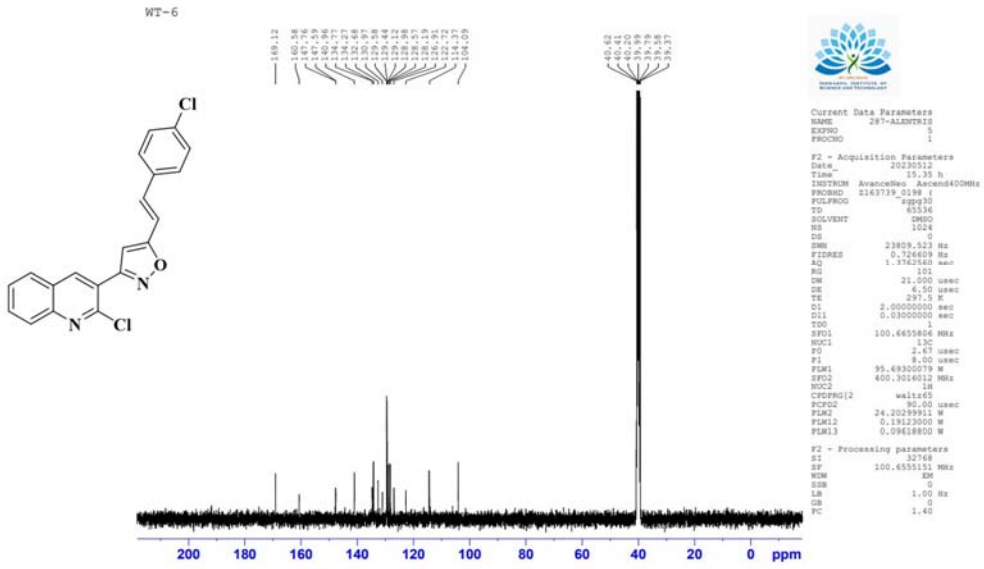

Figure 17: ^{13}C NMR spectra of compound **7f**

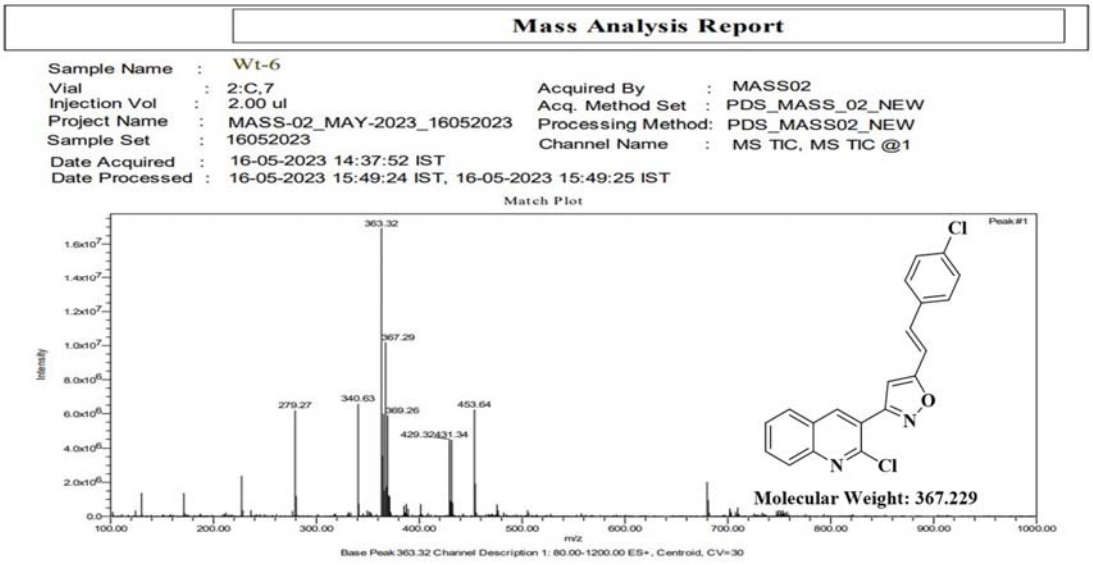

Figure 18: Mass spectra of compound **7f**

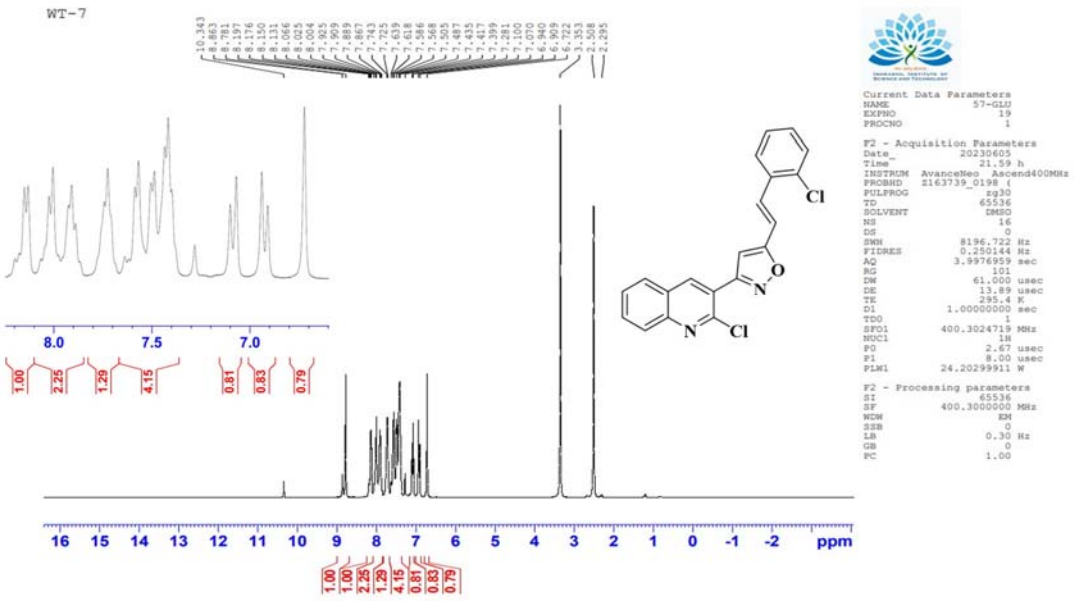

Figure 19: ^{1}H NMR spectra of compound **7g**

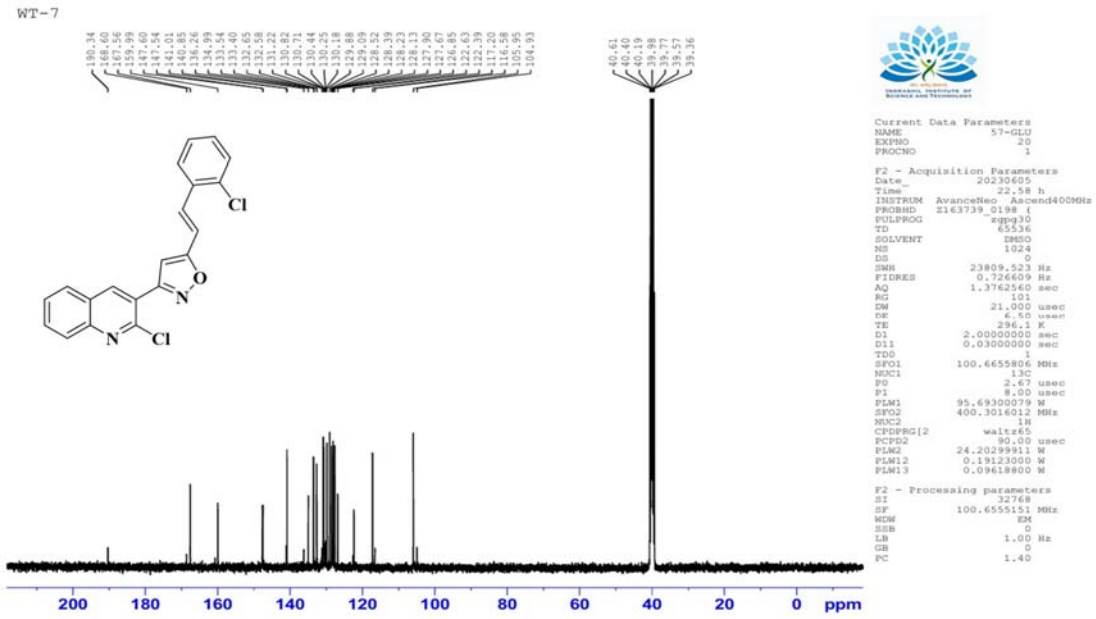

Figure 20: ^{13}C NMR spectra of compound **7g**

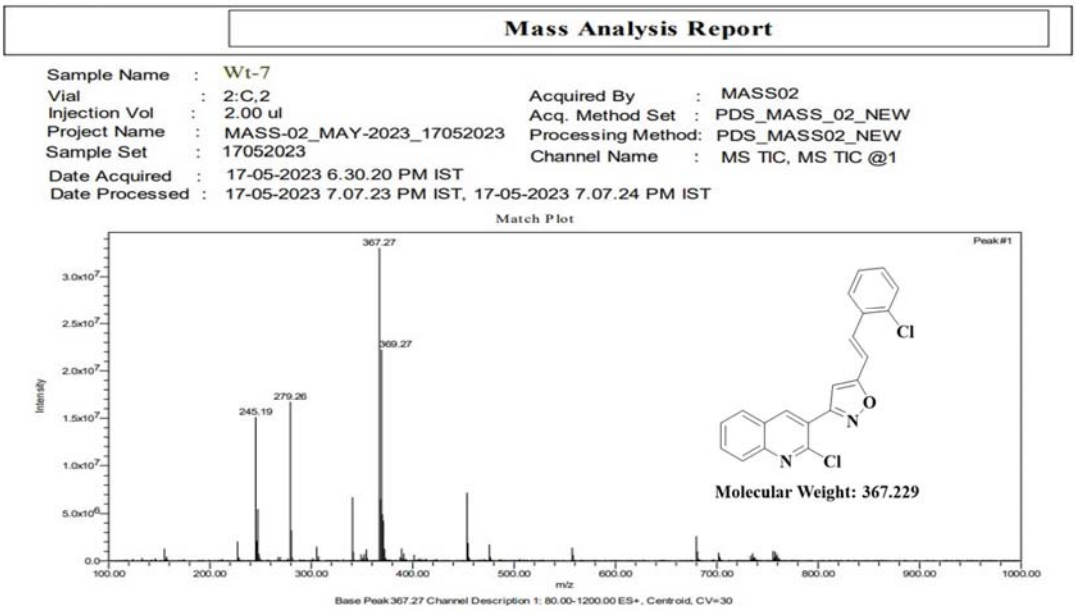

Figure 21: Mass spectra of compound **7g**

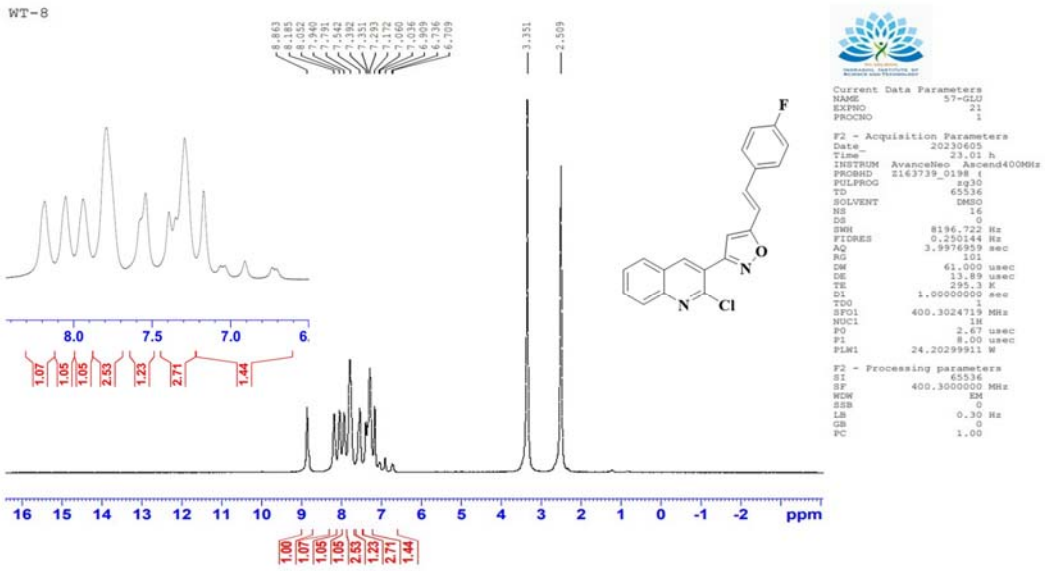

Figure 22: ^{1}H NMR spectra of compound **7h**

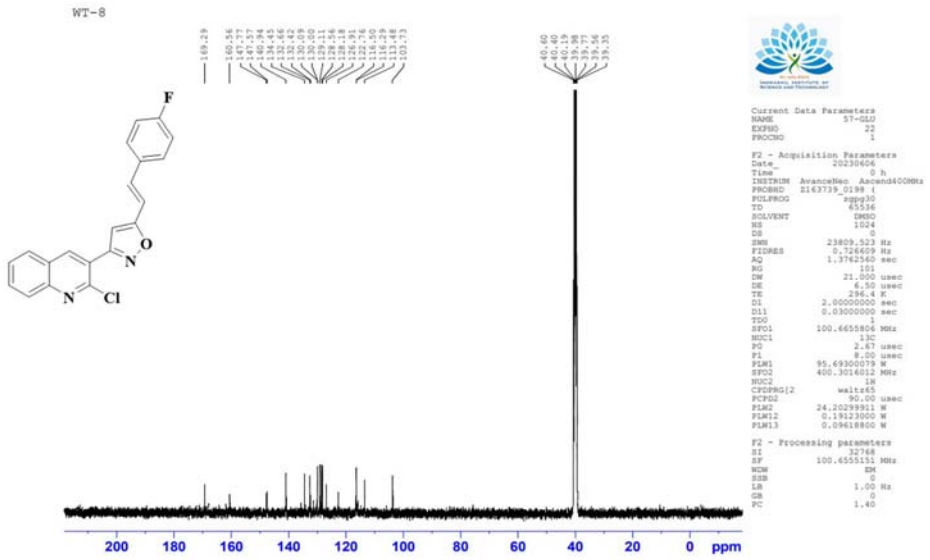

Figure 23: ^{13}C NMR spectra of compound **7h**

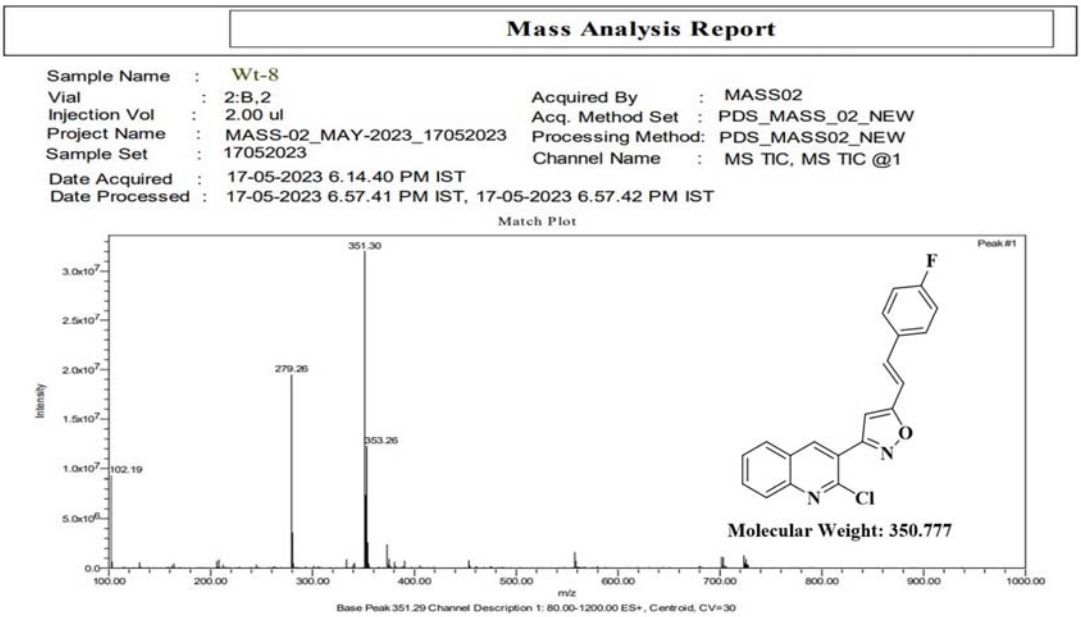

Figure 24: Mass spectra of compound **7h**

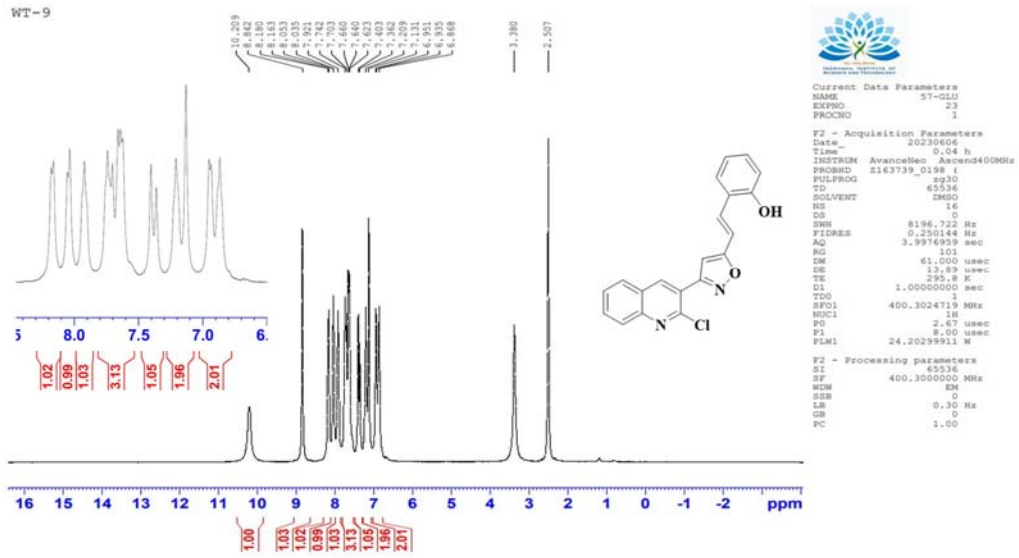

Figure 25: ^{1}H NMR spectra of compound **7i**

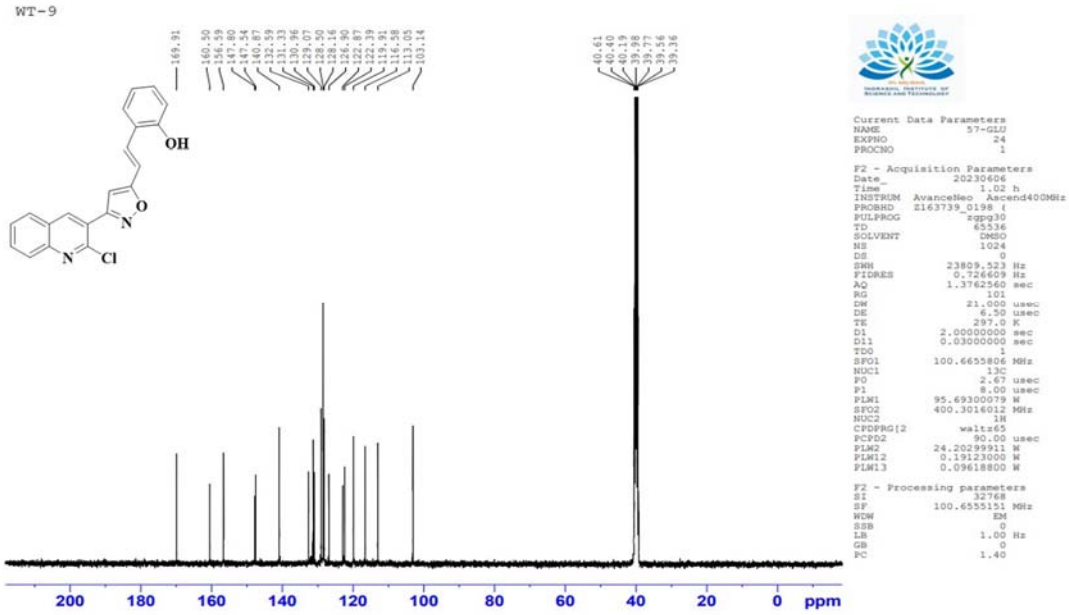

Figure 26: ^{13}C NMR spectra of compound **7i**

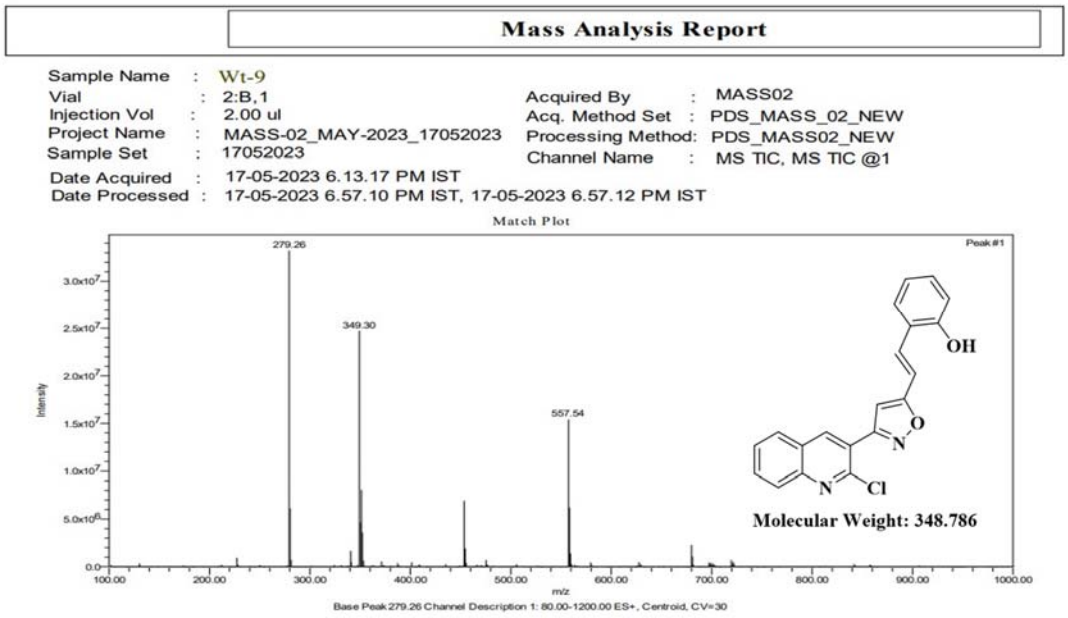

Figure 27: Mass spectra of compound **7i**

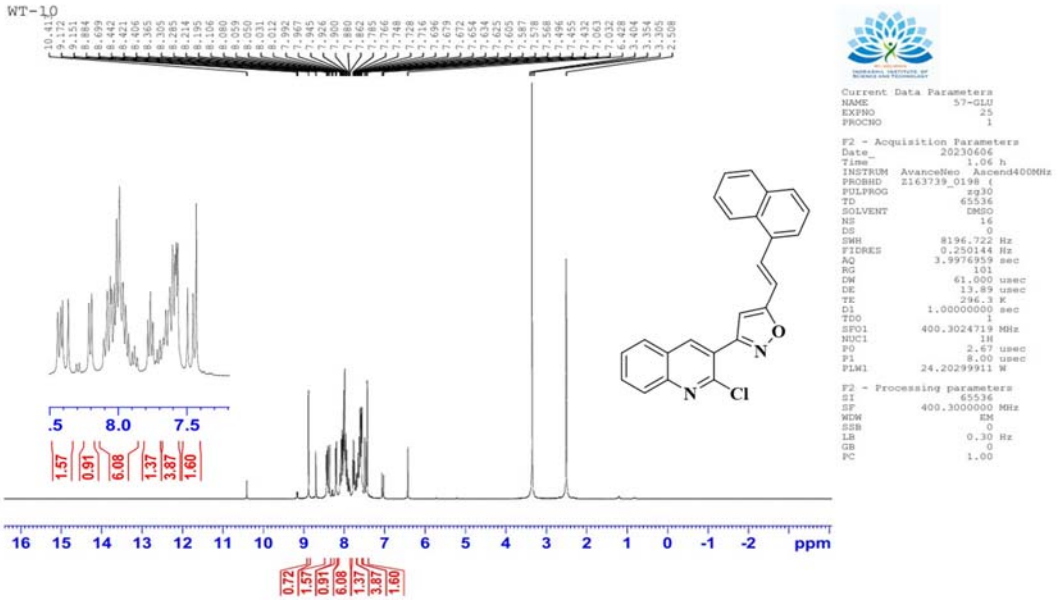

Figure 28: ^{1}H NMR spectra of compound **7j**

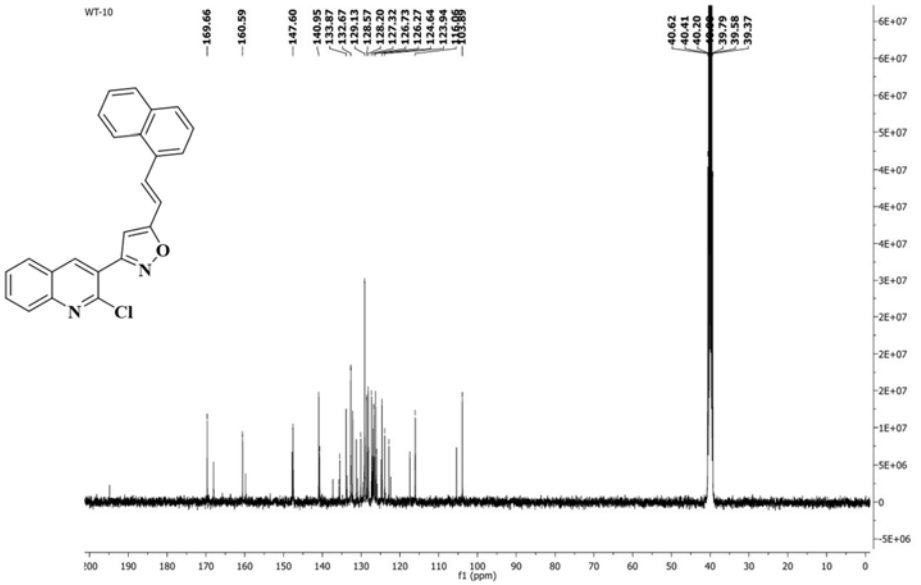

Figure 29: ^{13}C NMR spectra of compound **7j**

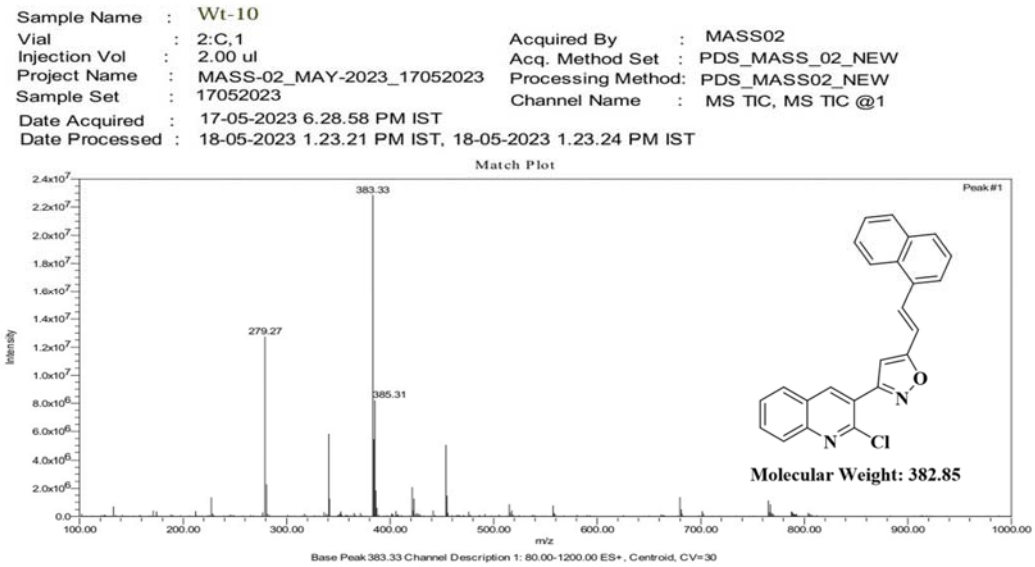

Figure 30: Mass spectra of compound **7j**

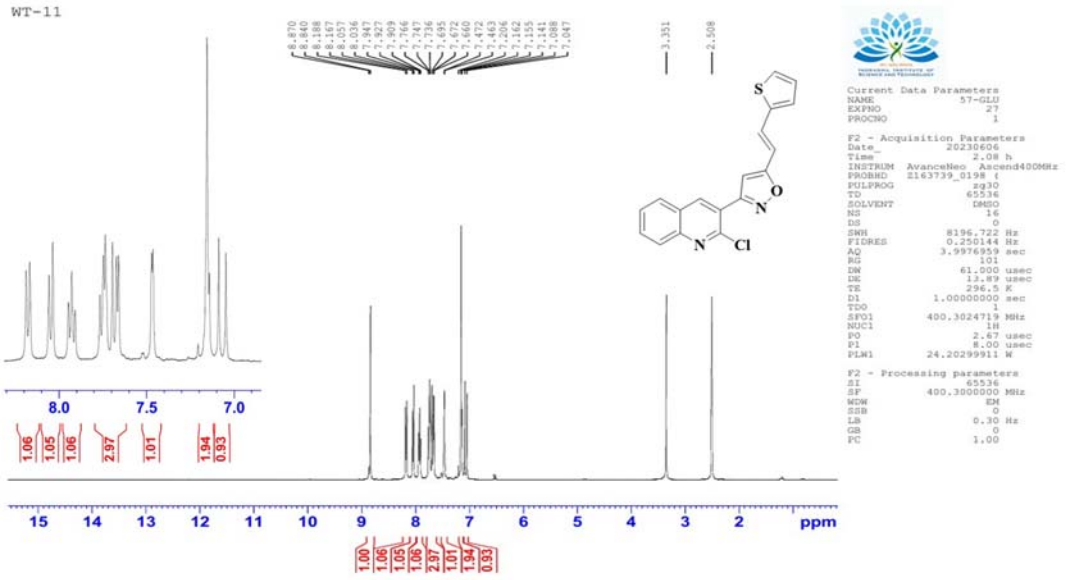

Figure 31: ^{1}H NMR spectra of compound **7k**

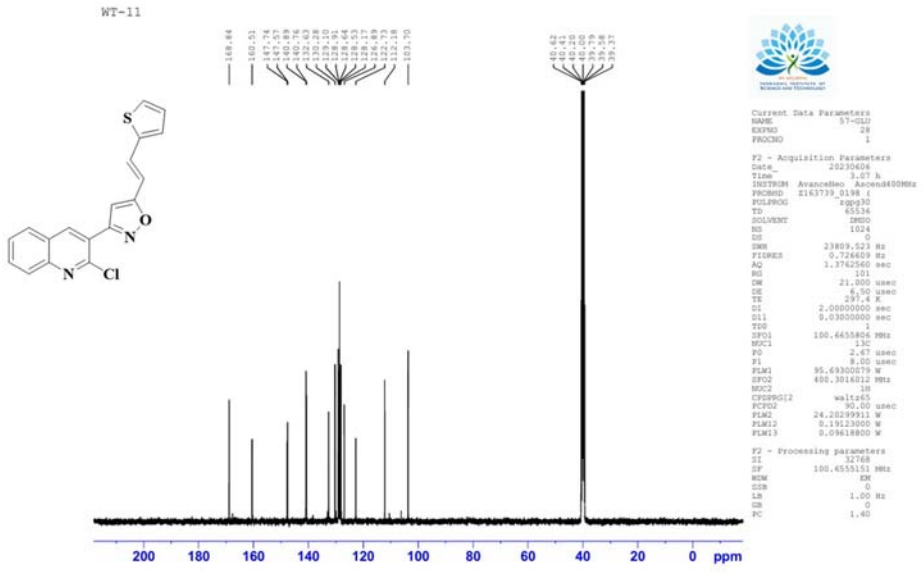

Figure 32: ^{13}C NMR spectra of compound **7k**

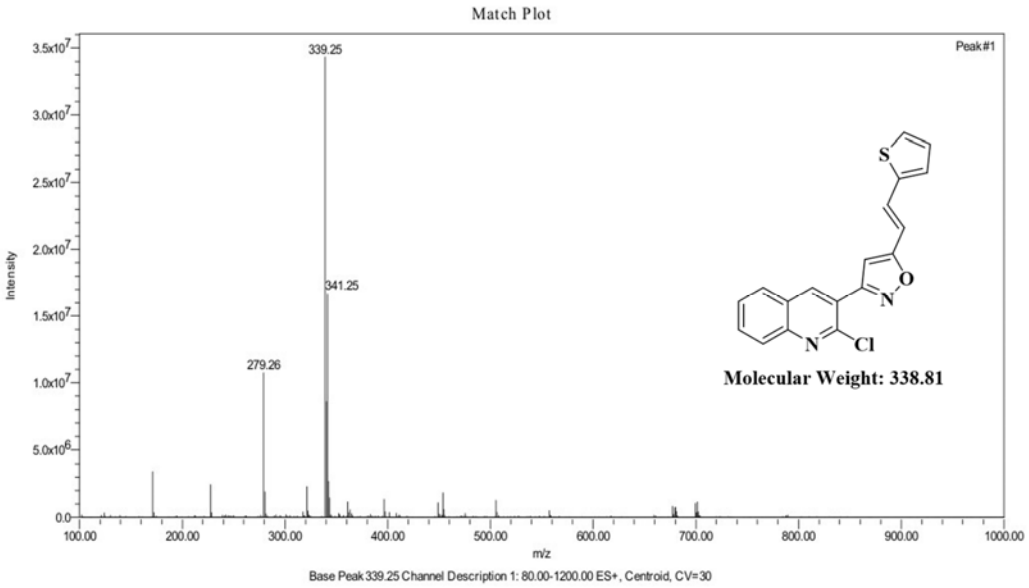

Figure 33: Mass spectra of compound **7k**

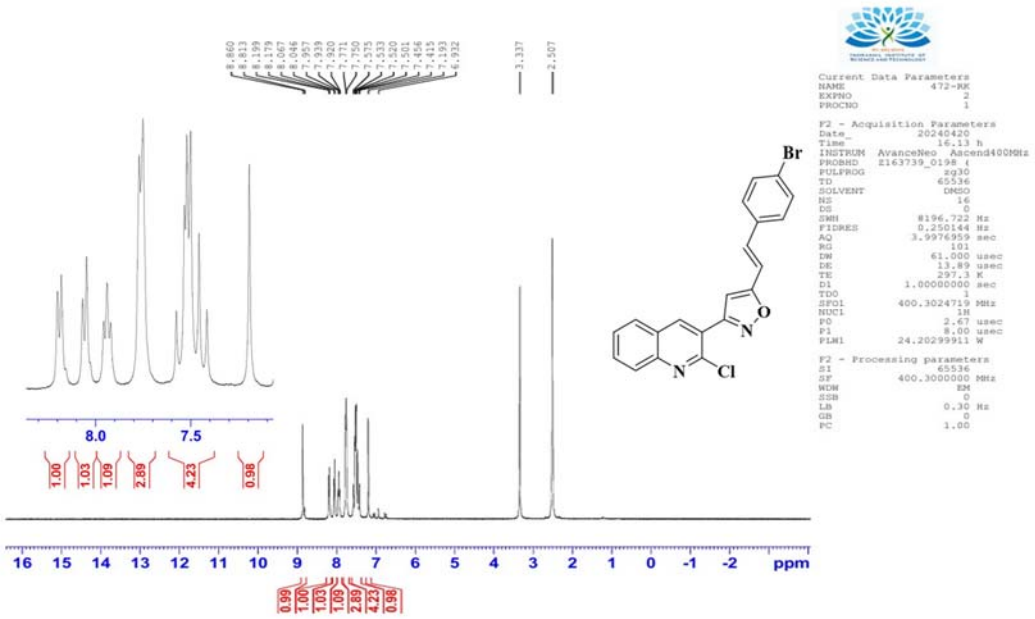

Figure 34: ^{1}H NMR spectra of compound **7l**

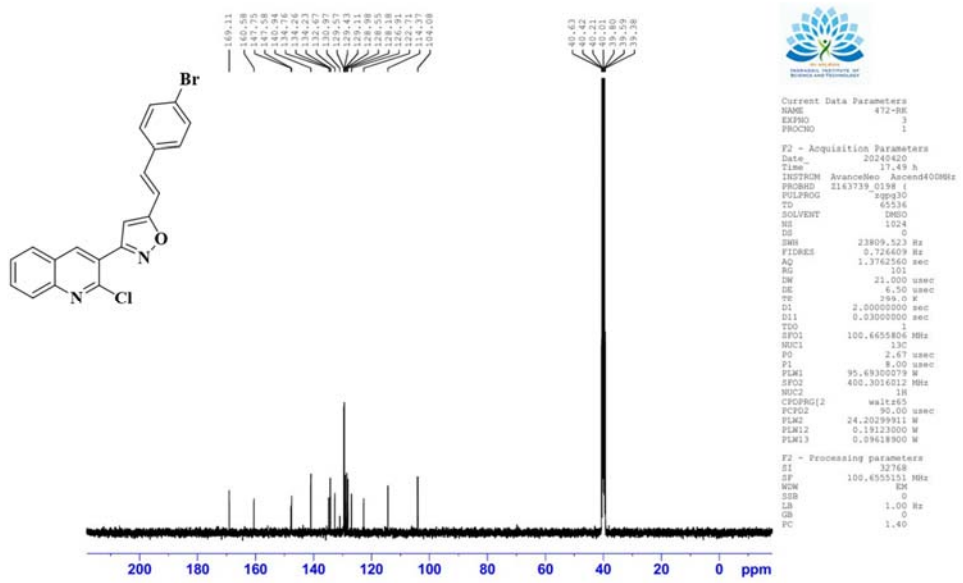

Figure 35: ^{13}C NMR spectra of compound **7l**

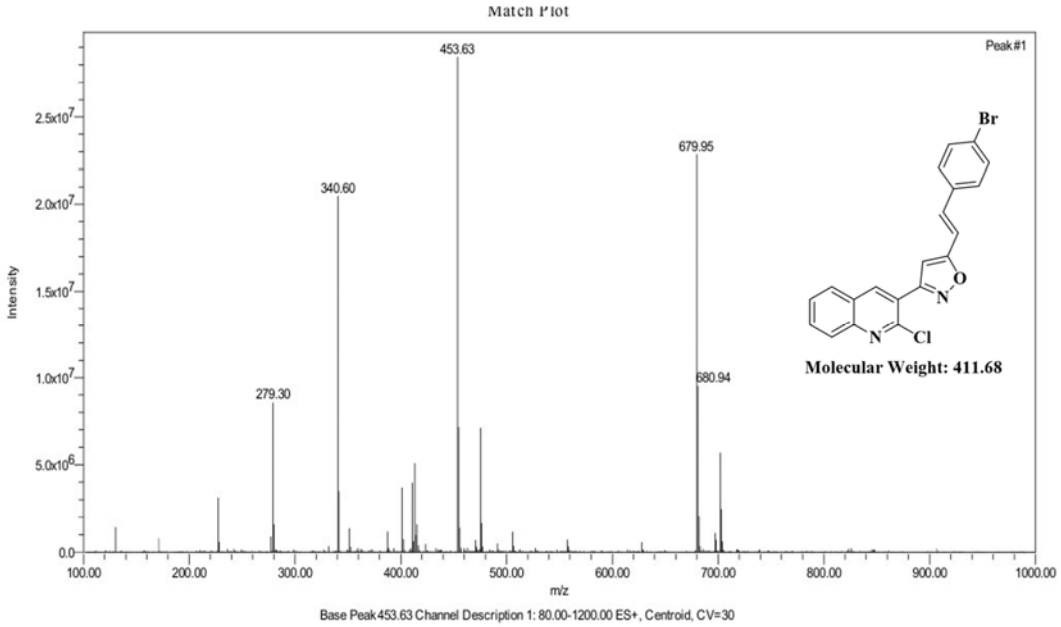

Figure 36: Mass spectra of compound **7l**